



# A review of molecular-beam epitaxy of wide bandgap complex oxide semiconductors

William Nunn<sup>1</sup>, Tristan K. Truttmann<sup>1</sup>, Bharat Jalan<sup>1,a)</sup> 

<sup>1</sup>Department of Chemical Engineering and Materials Science, University of Minnesota, Minneapolis, MN 55455, USA

<sup>a)</sup>Address all correspondence to this author. e-mail: bjalan@umn.edu

Received: 9 July 2021; accepted: 2 September 2021

Much progress has been made in the area of wide bandgap semiconductors for applications in electronics and optoelectronics such as displays, power electronics, and solar cells. New materials are being sought after and considerable attention has been given to complex oxides, specifically those with the perovskite crystal structure. Molecular-beam epitaxy (MBE) has come to the forefront of this field for the thin film synthesis of these materials in a high-quality manner and achieves some of their best figures of merit. Here, we discuss the development of MBE from its beginnings as a method for III–V semiconductor growth to today for the growth of many contenders for next-generation electronics. Comparing MBE with other physical vapor deposition techniques, we identify the advantages of MBE as well as many of the challenges that still must be overcome should this technique be applied to other up-and-coming wide bandgap complex oxide semiconductors.

## Introduction

Wide bandgap semiconductors are typically defined as those with bandgaps greater than 3 eV. These materials have been of great interest for application in power electronics and transparent conducting oxides due to their high dielectric breakdown strength and transparency in the visible spectrum, respectively [1–3]. Examples of materials within this category include the group III- and II-IV-nitrides (B, Al, Ga, In)N and (Zn, Mg, Cd) (Si, Ge, Sn)N<sub>2</sub>, the various polymorphs of SiC, and diamond. This category also includes binary oxides such as ZnO, TiO<sub>2</sub>, SnO<sub>2</sub>, GeO<sub>2</sub>, Ga<sub>2</sub>O<sub>3</sub>, and indium-doped tin oxide (ITO) as well as complex oxides such as SrTiO<sub>3</sub>, BaSnO<sub>3</sub>, SrSnO<sub>3</sub>, KTaO<sub>3</sub>, and KNbO<sub>3</sub>. These complex oxide wide bandgap semiconductors are of particular interest due to their structural and chemical compatibility with other complex oxides that serve other practical functions such as those of dielectrics (e.g., CaHfO<sub>3</sub>) and electrodes (SrRuO<sub>3</sub>) as well as those that show more exotic phenomena such as colossal magnetoresistance (La<sub>0.67</sub>Ca<sub>0.33</sub>MnO<sub>3</sub>) [4], high-temperature superconductivity (e.g., YBa<sub>2</sub>Cu<sub>3</sub>O<sub>7-x</sub>) [5], 3D Peierls transitions (BaBiO<sub>3</sub>) [6], multiferroicity (BiFeO<sub>3</sub>) [7], and metallic ferroelectricity (LiOsO<sub>6</sub>) [8]. This compatibility among such a diverse range of materials inspires a vision of integrating myriad functionalities into a single epitaxial monolithic

integrated circuit enabling technologies unavailable using traditional semiconductor technology.

This goal of monolithic function integration, however, puts stringent demands on the technique used to prepare complex oxide semiconductors. The technique should produce thin films with impeccable quality, ideally with control over single atomic layers. Furthermore, given the diversity of materials within this category, the technique should be highly versatile, allowing a single machine to grow many materials and switch between them nearly instantly. This allows for the growth of heterostructures to study how two or more materials behave when in contact. Finally, the technique should be modular, allowing the user to upgrade, modify, or adjust one component of the system with minimal impact on the other parts, allowing the researcher to systematically vary growth parameters without exorbitant recalibration requirements. Molecular-beam epitaxy (MBE) achieves all these goals, and is the topic of this review.

MBE is an ultra-high vacuum thin film growth technique which uses the co-deposition or shuttered growth of molecular beams containing the desired elements to form epitaxial films on a substrate. After developing a reputation for its ability to grow some of the highest quality films with atomic layer control, MBE has been used for the growth of a

wide variety of material systems with much success [9–14]. Here, we will focus on the extensive progress of MBE with focus on wide bandgap complex oxides of the perovskite crystal structure. Of these, SrTiO<sub>3</sub>, BaSnO<sub>3</sub>, and SrSnO<sub>3</sub> have been grown using MBE. SrTiO<sub>3</sub> is a quantum paraelectric with a bandgap of 3.2 eV [15], and an exceptionally high low-temperature mobility of 22,000 cm<sup>2</sup>V<sup>-1</sup>s<sup>-1</sup> in single crystals [16]. Although its room-temperature mobility is limited by phonons to less than 10 cm<sup>2</sup>V<sup>-1</sup>s<sup>-1</sup>, the treasure trove of phenomena available in this material including dilute superconductivity [17], two-dimensional electron gases (2DEG) with other oxides [18], and persistent photoconductivity [19] earn SrTiO<sub>3</sub> the title of being the most studied complex oxide.

Although SrTiO<sub>3</sub> has fascinated physicists since the 1960s, BaSnO<sub>3</sub> eluded attention until the 2010s when L-doped n-type single crystals were discovered to have a room-temperature mobility of 320 cm<sup>2</sup>V<sup>-1</sup>s<sup>-1</sup> at a carrier concentration of 8.0 × 10<sup>19</sup> cm<sup>-3</sup> [20, 21]. Such high conductivity with an indirect bandgap of ~3 eV [22] make BaSnO<sub>3</sub> appealing for room-temperature applications such as transparent electronics. The conduction band derived mostly of Sn 5s-orbitals [23], the resulting low effective mass of about 0.2 m<sub>0</sub> [24, 25], and weak electron-phonon coupling [26] which give BaSnO<sub>3</sub> these properties are also shared with the related material SrSnO<sub>3</sub>. However, SrSnO<sub>3</sub>'s ultra-wide bandgap (UWBG) of 4.1 eV [22] is appealing for application in UV-transparent electronics and high-power devices.

Here, after reviewing the history of physical vapor deposition and the development of oxide MBE, we discuss the inherent advantages of MBE and its various challenges for the growth of high-quality complex oxides. Then, we conclude by reviewing the growth of these three materials by MBE and discussing outstanding challenges for MBE to address in new materials systems.

## History of physical vapor deposition (PVD)

Tracing the history of thin film deposition can give us the context of where the field stands to today and where it is postured to go in the near future. Thin film deposition is typically divided into two categories: chemical vapor deposition (CVD), which involves chemical reactions occurring between volatile precursors, and physical vapor deposition (PVD), which involves the physical process of transporting sources between phases for film growth on a substrate. Here, we focus on PVD techniques which, through their progression (Fig. 1), have cemented themselves as instrumental in the development of wide bandgap complex oxide films.

As illustrated in Fig. 1, of the main PVD techniques, sputtering, thermal evaporation, MBE, and pulsed laser deposition (PLD), the first two found their inception over a century earlier than the latter two, in the 1850s [27]. The first published report of sputter deposition can be traced back to 1852 by Grove who observed the deposition of a film, primarily iron oxide, on a silver-plated substrate after creating an electrical potential between the substrate and a steel needle in low vacuum [28]. Although the term sputtering was not coined until years later, these experiments are the first observations of the phenomenon. The process of thermal evaporation was demonstrated a few years later by Faraday in 1857 who first “exploded” metal wires in a low vacuum, thereby thermally evaporating the sources to form a film [29]. What follow these early experiments is years of technological advancements, especially related to improving vacuum that eventually led to the more modern approaches that exist today.

Following these advancements, more than one hundred years later in the 1960s, the development of PLD and MBE began. PLD was first shown by Smith and Turner in a report published in 1965 in which they demonstrated, using a pulsed ruby laser, the deposition of a variety of materials, including semiconductors, chalcogenides, and dielectrics [30]. Their early work, although showing some mixed results, laid the foundation

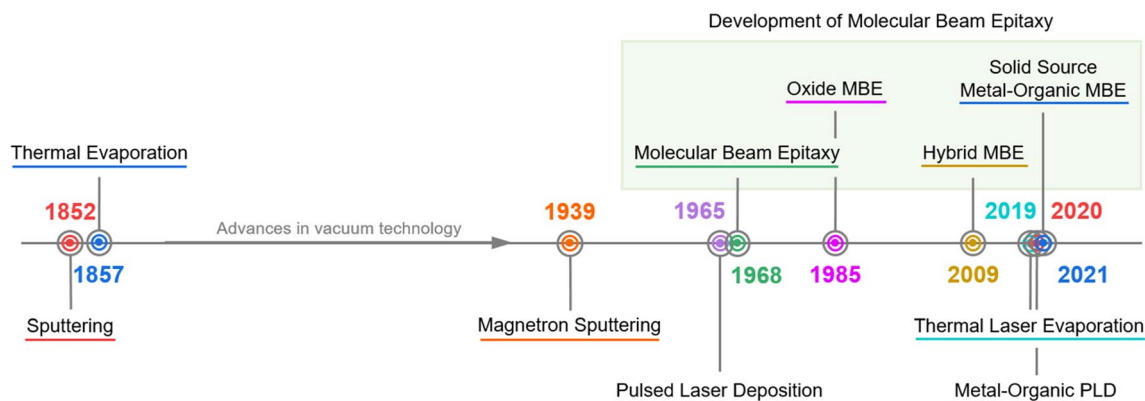


**Figure 1:** Timeline of the introduction of PVD techniques, including some of the modifications that have arisen with a focus on the development of MBE specifically.

for the much more refined technique widely used today. In fact, it played a key role in the development of high- $T_c$  superconductors in the late 1980s which flourished into a new ground-breaking field of study [5, 31–33]. Finally, MBE, derived from thermal evaporation, found its conception at Bell Labs by a group of scientists including John R. Arthur Jr who first published on the use of separate “molecular beams” of gallium and arsenic to form epitaxial GaAs films [34]. Alfred Y. Cho and others then joined him to develop the technique into what we call MBE today [35, 36].

Many advancements within these techniques have since been made including, importantly, magnetron sputtering [37] which has become the most common configuration of sputtering today. Within MBE [38, 39] and PLD [40], modifications include metal–organic-based approaches which substitute some metal–organic compounds for conventional metal sources.

## Development of MBE

As we will focus on throughout this review, MBE has played an important role in many materials science and physics discoveries as a result of both the conventional approach and the variations that have arisen. As shown in Fig. 2, MBE itself has rich history of scientific advancements since its inception in the late 1960s for the growth of III–V semiconductors like GaAs, as mentioned previously, with adsorption-controlled stoichiometric growth [34]. This control over the stoichiometry and consequently the structure of the films was enough to lead to the first demonstration of modulation doping in 1978 [41], which was previously unattainable due to the lower quality of films and heterostructures produced by other PVD techniques at the time. Within the following three years, the discovery of the integer and fractional quantum Hall effect was made as a result of these modulation-doped

heterostructures, which were the subjects of the Physics Nobel Prizes in 1985 and 1998 [42]. The 1970s and 1980s were then filled with rapid expansion of the MBE technique including for growth of II–VI semiconductors [43], III-nitrides [44], van der Waals epitaxy for 2D materials [45], and eventually the first report of MBE complex oxide growth, deposition of  $\text{LiNbO}_3$  in 1985 [46].

Although the first report of oxide MBE was for  $\text{LiNbO}_3$ , the field really took off following the 1986 discovery of high- $T_c$  superconductivity in cuprates [5]. Many researchers rushed to produce these materials as thin films and achieved incredibly rapid success. Following the first thin film cuprates grown by PLD [32], the first films were grown by MBE later the same year in 1987 [47, 48]. However, all these films required annealing in oxygen to show superconductivity. Indeed, the difficult oxidation of Cu to 3+ served as an early test of the limits of oxide MBE. But this challenge was overcome only one year later in 1988 with the development of pure ozone MBE which could produce superconducting films without post-annealing [49], and which was improved in 1990 with silica gel to prevent ozone explosions [50]. In this incredible span of 5 years, the field of oxide MBE went from conception to an accomplished technique attesting to the adaptability of the MBE approach.

Even as more reports of oxide MBE appeared, including the first demonstration of the high-mobility binary oxide ZnO [51–53], the problem of achieving cation stoichiometry in complex oxides still eluded researchers until the late 1990s when adsorption-controlled growth was first shown in oxide MBE [54–56]. Finally, in recent years, MBE has become prominent in the growth of topological materials like  $\text{Bi}_2\text{Se}_3$  [57, 58], room-temperature multiferroics [59], and low- [38] and room-temperature [60, 61] high-mobility oxide semiconductors which have included growth by the metal–organic-based modifications, like hybrid MBE.

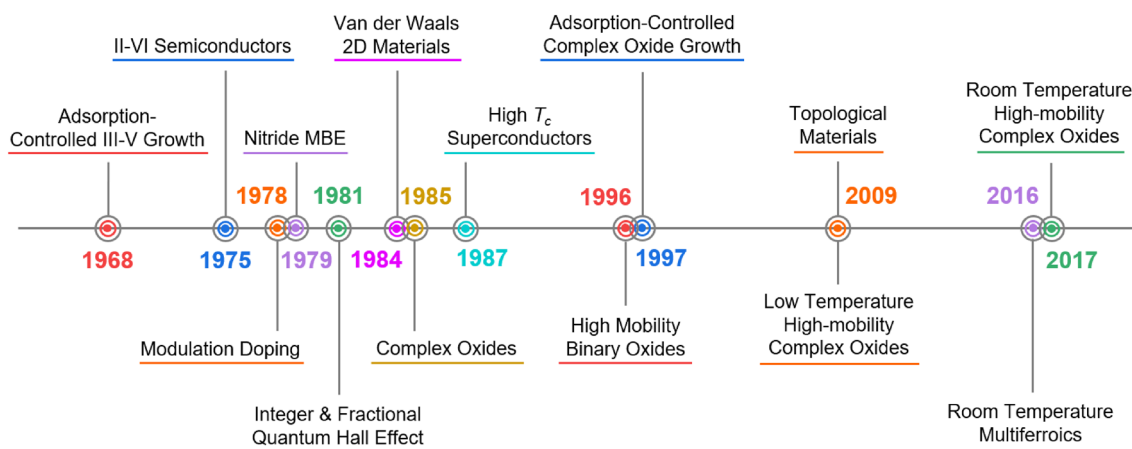


**Figure 2:** Timeline of the development of MBE for a variety of impactful classes of materials and discoveries.

## Technique comparison

Choosing a PVD technique is an exercise in comparing the advantages and disadvantages of each technique to the applications requirements and resources. These advantages and disadvantages are summarized in Table 1. CVD and sputtering have found a lot of success in larger-scale industrial processes due to their simplicity, lower costs, and, especially with sputtering, high scalability. However, it is a different story when it comes to developing new materials on a research level, especially with complex oxides. In this environment where sample quality and material flexibility are valued over scalability, PLD and MBE have become the predominant thin film growth techniques.

A key factor for developing new materials and revealing their underlying physics is the defect concentration of the material. While defects can prove useful and have led to numerous studies on defect engineering [62], unintentional defects tend to impede our ability to study the intrinsic properties, in particular with wide bandgap semiconductors. Here, we will discuss two deposition parameters that are crucial to understanding defect formation in PVD techniques: particle kinetic energies and mean free path.

Of all the different deposition parameters, perhaps none is more important to understand defect formation than kinetic energy of the vapor phase atoms or molecules as they interact with the growth front. Although high incident particle energy can be exploited, such as for orientation-selective resputtering for the growth of fully oriented films on amorphous substrates [63], high-energy particles are usually regarded as a nuisance. Under high fluences, high particle energies can lead to resputtering of film constituents resulting in the non-stoichiometry defects discussed below [64]. The particles can also impact and sputter components in the vacuum chamber

leading to the incorporation of unintentional impurities. However, even at low fluences, high particle energies can lead to non-equilibrium intrinsic point defects such as oxygen and cation vacancies, interstitials, and anti-site defects which can all negatively impact material properties, even in small concentrations. High-energy techniques such as sputtering and PLD tend to form higher concentrations of point defects in films, whereas low-energy thermal techniques like MBE produce fewer defects. In principle, the use of oxygen plasmas could introduce high-energy particles into the growth chamber, but simple measures like deflection plates minimize their detrimental effects on growth.

The mean free path of the deposition process also plays a role in defect formation. The mean free path ( $\lambda$ ) is calculated as

$$\lambda = \frac{kT}{\sqrt{2}\pi d^2 P}, \quad (1)$$

where  $k$  is Boltzmann constant,  $T$  is temperature,  $d$  is the kinetic diameter of atom or molecule, and  $P$  is the pressure. As shown, the mean free path is inversely proportional to pressure. In MBE, the mean free path exceeds the source-substrate distance by an order of magnitude or more. Thus, source species do not interact during transport from the source to the substrate. This eliminates the possibility of parasitic chemical reactions that can cause unintentional aerosol formation in low-vacuum techniques such as low-pressure chemical vapor deposition (LP-CVD). The high mean free path of MBE also limits deposition species to only those that originate from the surfaces in direct line of sight to the substrate. By using high-purity source material, high-temperature system bakeouts, and cryogenic cooling shrouds to limit surface outgassing, MBE can achieve extremely low impurity levels even when one reactor is shared among multiple material systems. These two advantages

**TABLE 1:** Advantages and disadvantages of conventional PVD techniques as well as two of the metal–organic-based MBE variations.

Technique	Advantages	Disadvantages
Magnetron sputtering	High deposition rate and scalability. Able to supply many metals and dielectrics. Ease of use for ultra-low vapor pressure metals compared to evaporation techniques	Stoichiometry of target is not necessarily transferred to film. High energy can lead to defect nucleation. Backsputtering of deposited films if not using off-axis
Pulsed laser deposition	Flexibility in laser wavelength and power. Precise growth rate control. Stoichiometric target transfer is capable in many cases. Ease of use. <i>In-situ</i> characterization available, e.g., RHEED	Stoichiometry of target is not necessarily transferred to film. High energy can lead to defect nucleation
Conventional oxide MBE	Excels at limiting defects due to low-energy deposition. Adsorption-controlled stoichiometric growth is possible for some materials. Monolayer growth control. <i>In-situ</i> characterization available, e.g., RHEED	Stoichiometry limited by degree of flux control if no growth window. Oxygen stoichiometry and metal oxidation limited by low oxygen background pressure. Source oxidation. Low growth rates
Hybrid MBE	Great control over stoichiometry due to growth windows. No source oxidation of metal–organic. Can supply oxygen and pre-oxidized metal via metal–organic precursors	High vapor pressure and thermally stable metal-organics required. Need external vapor inlet system
Solid source metal–organic MBE	Able to supply elements having ultra-low vapor pressures with source temperatures < 200 °C. Possible to supply “pre-oxidized” elements. No vapor inlet needed. No source oxidation of metal–organic. Cheap and safe	Must use solid and thermally stable metal-organics with intermediate vapor pressures. Cannot fully bake system due to metal–organic source. Potential contamination if the room-temperature vapor pressure is non-negligible

make MBE highly advantageous for the fundamental study of new materials. Finally, whereas low-vacuum techniques like LP-CVD require the chamber's residence time to stop depositing one material and begin depositing another by pumping out one precursor and replacing it with another [65], the high mean free path of MBE allows the use of shutters to make this switch nearly instantaneous, limited only by the speed of the shutter. This makes MBE the method of choice to grow heterostructures that demand highly abrupt interfaces, even in commercial devices such as Hall effect sensors and high-electron mobility transistors. This ability to rapidly switch between two materials has also been exploited to grow non-equilibrium structures such as high-index Ruddlesden–Popper phases [66–72].

In PVD techniques with high particle energies, however, lower mean free paths can offer the advantage of lowering the particle energies through collisions with ambient gas molecules. This is the main motivation behind development of high-pressure oxygen sputtering which has been applied to cuprate superconductors [73, 74],  $\text{La}_{1-x}\text{Sr}_x\text{MnO}_3$  [75],  $\text{PbZr}_x\text{Ti}_{1-x}\text{O}_3$  [76], amorphous  $\text{GdScO}_3$  on Si [77],  $\text{BaTiO}_3$  [78],  $\text{SrTiO}_3$  [79], and  $\text{BaSnO}_3$  [80–82].

The high vacuum of oxide MBE also offers the advantage of a high mean free path for electrons and ions required for in-situ materials characterization. Most research MBE systems use concurrent reflection high-energy electron diffraction (RHEED) to monitor the growth in real time, but in-situ characterization of MBE films has also been done with low-energy electron diffraction (LEED), low-energy electron microscopy (LEEM) [83], X-ray photoelectron spectroscopy (XPS) [84, 85], Auger electron spectroscopy (AES) [86, 87], and scanning electron microscopy (SEM). The use of vacuum suitcases also allow samples grown by MBE to be transferred to distant characterization equipment—such as synchrotron facilities—without exposure to air [88].

### Cation stoichiometry control

The advantages outlined for MBE show great inherent potential for the technique; however, the method is not without challenges. Perhaps, the most significant challenge for MBE is control over stoichiometry. Because MBE relies on the co-deposition or shuttered growth of individual elements, achieving cation stoichiometry is a major challenge, especially in semiconductors where small levels of non-stoichiometry can render a device useless. For example, in a prototypical oxide semiconductor  $\text{SrTiO}_3$ , where Sr vacancies serve as acceptors, even a 0.1% drop in Sr flux would result in an acceptor concentration of  $\sim 2 \times 10^{19} \text{ cm}^{-3}$ , enough to fully compensate even moderate doping concentrations. Although progress has been made using beam flux monitors (BFM), quartz crystal microbalances (QCM), atomic absorption spectroscopy (AAS) [89],

electron-impact-emission spectroscopy (EIES) [90–92], and RHEED [93, 94] to fine-tune fluxes—many of them in real time—these techniques all involve errors around 0.1–1% under ideal conditions [89, 93, 95], and perhaps, much larger errors under realistic conditions.

The obstacle of stoichiometry was first overcome for the growth of III–V semiconductors by exploiting thermodynamics to self-regulate the stoichiometry. Figure 3a shows the thermodynamic equilibrium curves for the two reactions that can regulate the stoichiometry of GaAs [55]. As shown, at relatively low growth temperatures, there exists a large range of As vapor pressures within which the stoichiometry is self-regulated. This range of pressure as a function of substrate temperature is referred to as a “growth window.”

However, the concept of a MBE growth window was not demonstrated in oxides until decades later in the late 1990s [54–56, 96]. Figure 3b shows the growth window of one of these early systems,  $\text{PbTiO}_3$  and how the range of vapor pressures—spanning about 2 orders of magnitude—is considerably smaller than that of GaAs which spans about ten orders of magnitude [55]. In practice, this made the stoichiometric growth of  $\text{PbTiO}_3$  feasible. Adsorption-controlled growth of other complex oxides using oxide MBE have since been found for a variety of materials [13], but these windows are usually smaller than in GaAs and occur at higher temperatures.

Still, many complex oxides lack the volatile species necessary to support a growth window at realistic growth conditions. For example,  $\text{SrTiO}_3$  lacks a sufficiently volatile constituent which makes the calculated growth window occur at very high growth temperatures or unreasonably low SrO vapor pressures, as shown in Fig. 3c [97]. Thus, without a growth window, the stoichiometry of  $\text{SrTiO}_3$  could only be as good as the control over the Sr and Ti fluxes. Given the difficulty of evaporating Ti, due to its low vapor pressure and the tendency of both Sr and Ti to oxidize at the source [98, 99], this control was quite poor. Growing  $\text{SrTiO}_3$  with sufficiently low defect concentrations to be a useful oxide semiconductor was not feasible. Efforts have been made to combat the low vapor pressure and source oxidation by supplying Ti with a Ti-sublimation pump known as Ti-Ball [98]. Although  $\text{SrTiO}_3$  films have been grown with high structural quality, stoichiometry control with traditional MBE is not sufficient to support robust semiconductor-like doping.

It was not until the hybrid MBE approach was developed that  $\text{SrTiO}_3$  films could be grown with MBE having a sufficient degree of stoichiometry control to support chemical doping. Using titanium(IV) tetraisopropoxide (TTIP), a metal–organic precursor to supply Ti, it was first shown that a MBE growth window can exist for  $\text{SrTiO}_3$  due to the high volatility of this precursor [97]. A large growth window in terms of the Sr/TTIP flux ratio was demonstrated, and stoichiometric materials could be obtained in a highly reproducible manner. Due to this control of

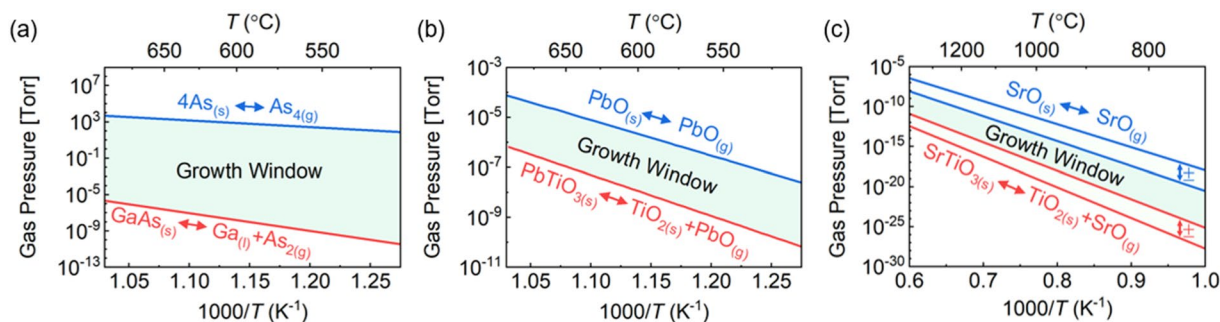


**Figure 3:** Adsorption-controlled MBE growth windows governed by the thermodynamic equilibrium curves if elemental sources are used for (a) GaAs, (b) PbTiO<sub>3</sub>, and (c) SrTiO<sub>3</sub>. Two sets of lines for both reactions are shown in the case of SrTiO<sub>3</sub> due to uncertainty in the thermodynamic data. Reproduced with permission [55, 97].

the stoichiometry and the low-energy aspect of MBE growth, a record low-temperature electron mobility has been achieved, even surpassing those of bulk single crystals. Electron mobility from MBE-grown films are now almost an order of magnitude larger than other techniques, with values of around 53,000 cm<sup>2</sup>V<sup>-1</sup> s<sup>-1</sup> at 2 K [100] compared to 6600 cm<sup>2</sup>V<sup>-1</sup> s<sup>-1</sup> by PLD [101].

Since the first report of hybrid MBE, the use of metal-organic precursors for the adsorption-controlled growth of other perovskite oxides have been shown for other titanates [102–104], vanadates [105], and stannates [106, 107]. Figure 4a shows the out-of-plane lattice parameters for one of these systems, BaSnO<sub>3</sub>, as a function of the A- to B-site flux ratios [108]. Typically, what is seen, as shown here, is a constant out-of-plane lattice parameter within the growth window signifying stoichiometric growth. It should be noted, however, that lattice parameter is itself not a direct measurement of composition and the sensitivity of X-ray diffraction to cation stoichiometry is limited to no better than ~1%. Carrier mobility is a more sensitive measure. Evidence of cation stoichiometry in BaSnO<sub>3</sub> can be further seen in Fig. 4b by enhanced electron concentration and mobility inside the growth window due to a decrease in compensating non-stoichiometric-related defects.

As a final note, it may also be possible to use thermal laser substrate heating to open up growth windows in some of these oxides systems by heating substrates up to incredibly high temperatures for growth. Looking at Fig. 3c again, as the growth temperature is increased, the SrO vapor pressure needed will eventually reach feasible levels. By using a laser, for example, a CO<sub>2</sub> laser, for substrate heating, substrate temperatures greater than 1500 °C have been demonstrated [109].

### Oxidation and anion stoichiometry

Another challenge with oxide MBE is to fully oxidize the cations and to achieve oxygen stoichiometry. Figure 5 shows the standard oxidation potentials ( $E_0^{\text{ox}}$ ) of select elements which

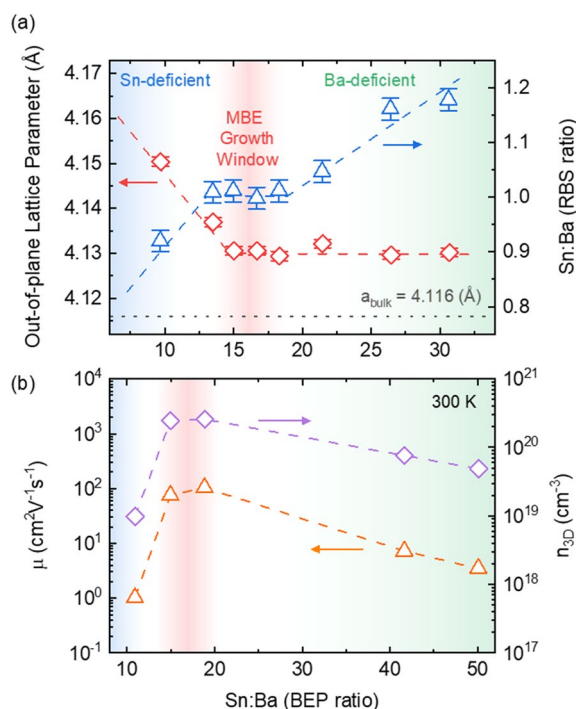


**Figure 4:** (a) Out-of-plane lattice parameter (left axis) and Sn:Ba atomic ratio from RBS (right axis) in hybrid MBE-grown BaSnO<sub>3</sub> films. (b) Room-temperature electron mobility (left axis) and carrier concentration (right axis) showing the enhanced electronic properties within the adsorption-controlled MBE growth window. Reproduced with permission [108].

are commonly used or sought after in complex oxide growth [110]. In some materials, especially transition metal-based perovskites like SrTiO<sub>3</sub>, insufficient oxidation of one cation (in this case forming Ti<sup>3+</sup> rather than Ti<sup>4+</sup>) may lead to films with good structural quality, but high carrier concentrations due to oxygen vacancies serving as shallow donors [16, 111]. Although this can be exploited for donors in the absence of chemical dopants, it is usually preferable to achieve full oxygen stoichiometry. For example, in dielectric and ferroelectric oxide systems, oxygen

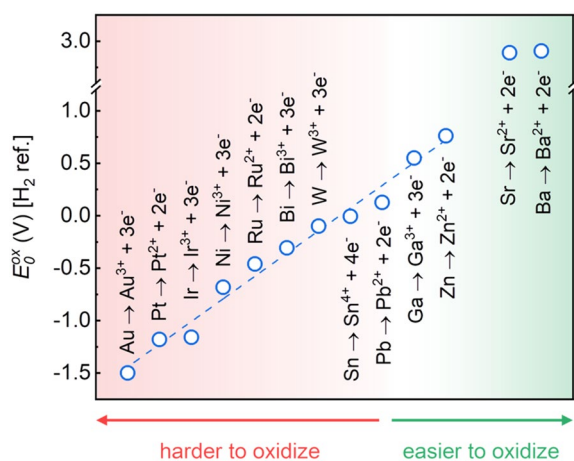


**Figure 5:** Standard oxidation potentials referenced to the standard H<sub>2</sub> electrode for select metals [110] which are commonly used or sought after in MBE growth. Metals are ordered from harder to oxidize to easier to oxidize, left to right. Dashed line is a guide for the eye.

vacancies can cause considerable leakage currents and, therefore, negatively impact material and device properties [112]. In other materials, especially main-group metal-based perovskites like BaSnO<sub>3</sub>, insufficient oxidation of one cation (Sn<sup>0</sup> or Sn<sup>2+</sup> rather than Sn<sup>4+</sup>) can be so severe as to ravage film quality altogether. For example, attempts to grow BaSnO<sub>3</sub> in inadequate oxidizing environments have resulted in the formation of ostensible liquid tin metal droplets on the substrate during deposition [113]. In less severe cases of incomplete oxidation, BaSnO<sub>3</sub> also forms oxygen vacancies that act as shallow donors [80, 114]. This diverse range of oxidation-related phenomena in BaSnO<sub>3</sub> makes it an excellent case study of oxidation in MBE.

Two crucial factors which impact the oxygen stoichiometry in oxide MBE are the choice of oxidant and the oxidant background pressure. However, the background pressure is usually limited to below 10<sup>-4</sup> Torr by the mean free path constraints of MBE [115], so we will only discuss the choice of oxidant. While molecular oxygen (O<sub>2</sub>) has been used in early oxide MBE, its oxidizing power is not sufficient in many cases, notably requiring post annealing to grow high-*T<sub>c</sub>* superconductors [48]. A common solution to achieve a more aggressive oxidizing environment at the same background pressure is to activate the oxygen using inductively coupled plasma (ICP) which creates up to a few percent of highly reactive dissociated oxygen atoms [38, 116, 117]. For an even more aggressive oxidizing environment, electron cyclotron resonance (ECR) plasma can be used [84, 118, 119], which can achieve a dissociation fraction exceeding twenty percent [120]. Another option is to generate ozone (O<sub>3</sub>) and then, optionally, distill it to generate up to 100% ozone before it enters the vacuum chamber [49]. Distilling ozone presents the potential hazard of explosions from its rapid decomposition, but this risk can be mitigated by distilling it over the high surface area offered

by silica gel to prevent percolation of the liquid [50]. However, challenges still remain with the operation of an ozone distiller and maintaining a stable ozone flow into the deposition chamber.

Other oxidants have also been experimented with. Both nitrogen dioxide (NO<sub>2</sub>) and hydrogen peroxide (H<sub>2</sub>O<sub>2</sub>) are noteworthy for being aggressive oxidants with relatively low vapor pressure; easily absorbed onto cryo-shrouds, they can achieve low background pressures even with high beam equivalent pressures [121, 122].

Even with these aggressive oxidizing species, the limited background pressures available in MBE may be insufficient to achieve full cation oxidation. One route to overcome this limitation is to supply oxygen bonded to one of the metal sources. This can be simply done by supplying the oxide of the metal, for example SnO<sub>2</sub> for the growth of BaSnO<sub>3</sub> [60, 113] and SrSnO<sub>3</sub> [123], or supplying the oxygen via the organic ligands in metal-organics as is done in hybrid MBE [38]. Using this second approach, it has been shown that high-quality SrTiO<sub>3</sub> films can be grown using only TTIP and no separate oxygen source, albeit with oxygen vacancies [124]. Alternatively, the ligand can be designed with reactivity toward oxygen sources. In a technique variation called “radical-based” hybrid MBE, Sn is supplied via the chemical precursor hexamethylditin (HMDT). At the growth front’s elevated temperatures, the weak Sn–Sn bond at the center of the molecule is argued to undergo homolytic cleavage affording trimethyltin radicals. These radicals react aggressively with oxidizing species, allowing the full oxidation of Sn even when unactivated molecular oxygen is used as the oxidant [106]. The organometallic HMDT has been used to grow stoichiometric films of both BaSnO<sub>3</sub> [61, 106, 108] and SrSnO<sub>3</sub> [107, 125–127] with growth windows present, shown in Fig. 4 for BaSnO<sub>3</sub>.

### Source oxidation

While a major challenge for early oxide MBE was to fully oxidize low-oxidation-potential metals such as Cu, there was a seemingly conflicting goal of preventing oxidation of high-oxidation-potential metals such as Y before they leave their crucible. This problem coined “source oxidation” can alter the fluxes of these metals during growth, worsening the flux instabilities and non-stoichiometry discussed above [98, 128]. A signature of such source oxidation is the need for higher source temperature to obtain the same flux reaching to the point when there is no flux beyond which a refill becomes required. One early strategy to combat source oxidation is to produce an oxidant pressure gradient across the chamber [49]. Baffles are added to separate the substrate and source regions of the chamber, with holes only large enough for the metal fluxes to reach the substrate. The oxidant is supplied centimeters away from the substrate while the

two regions of the chamber are differentially pumped. This strategy provides a high oxidant pressure immediately surrounding the substrate where it is needed and a much lower pressure near the sources where it is unwelcome. However, less extreme chamber design choices can also be implemented to lessen source oxidation. For example, extending the effusion cell port length will cause deposition of metal on the port walls between the effusion cell and the main chamber. These deposits can get oxidizing species, minimizing the quantity that reaches the crucible [99]; narrowing the effusion cell port will enhance this effect [129]. Choosing a crucible with a small orifice or adding an aperture to the crucible can also slow the ingress of oxygen and improve flux stability [3, 130].

Despite the advancements, these strategies all only lessen the effects of source oxidation; they do not solve it entirely. There are two strategies that thoroughly eliminate the problem of source oxidation by delivering the metal in a different chemical form. One way is to inject the element into the chamber in the form of a gaseous precursor, as done in hybrid MBE [38]. Regardless of the reactivity between the precursor and oxidizing species, the two do not interact until they are absorbed on the growth front. Hybrid MBE uses an effusion cell to supply the second metal element in complex oxide growth that can often be prone to source oxidation. However, any resulting flux instabilities ideally remain within the wide growth window that hybrid MBE affords. The second strategy is to evaporate the metal from an effusion cell in a form that does not react with oxygen. This can be a simple metal oxide, such as  $\text{SnO}_2$  [113], or an air-stable precursor such as  $\text{Ru}(\text{acac})_3$  or  $\text{Pt}(\text{acac})_2$  discussed below [39].

### Stubborn metals: where ultra-low vapor pressures meet ultra-low oxidation potentials

MBE often uses refractory metal filaments and crucibles to heat and contain transition metals during their high-temperature sublimation. This begs the question: how can one supply a refractory metal itself for MBE growth? Rather than uniformly heating an entire source load and crucible, a well-developed strategy is to use a focused energy beam that locally heats the source material to extremely high temperatures without drastically increasing the temperature of the crucible. The high-energy beam has historically been one of electrons, and is referred to as “electron-beam” evaporation [84], but the new and exciting “thermal laser evaporation” techniques use a continuous laser mounted outside the vacuum chamber [131]. Focusing on the conventional method, electron-beam systems can be much more expensive than effusion cells, the required high voltage presents safety risks, the instrument operation can produce RF noise that interferes with other equipment [132], the flux stability is poor, and some metals are prone to spitting. Finally, electron-beam evaporation can

be operationally complex, requiring monitoring and periodic electron-beam alignment to avoid accidental crucible evaporation after source depletion.

Related to refractory metals, the Pt group is a set of metals that are not only extremely low in vapor pressure but also among the hardest metals to oxidize. Complex oxides containing Pt-group and refractory metals include ruthenates, iridates, tungstates, and Pt-group delafossites. A few of these materials have been grown using MBE with electron-beam evaporation and strong oxidants [133–135]. However, the above-mentioned challenges with electron-beam evaporation merit a search for an easier way to grow these materials with potentially higher quality. To address these issues, the authors recently developed solid-source metal–organic MBE. This approach uses a low-temperature effusion cell to directly sublime solid metal–organic materials containing Pt-group metals in a pre-oxidized state [39]. This approach has facilitated the deposition of Pt-group metals and metal oxides with effusion cell temperatures less than 100 °C. Early successes include the growth of the simple metal Pt, binary oxide  $\text{RuO}_2$ , and the complex oxide  $\text{SrRuO}_3$  using only ICP as an oxidant, whereas the stronger oxidant of distilled ozone had previously been used for these oxides [135–137]. Significantly, this method potentially reaps the other benefits of hybrid MBE without the need for complex external vapor inlet systems.

### Choosing precursors

The choice of solid metal–organics discussed here or liquid metal–organics used in hybrid MBE warrants a brief overview of the general requirements for choosing a precursor in these metal–organic-based approaches. Hybrid MBE, due to supplying precursor through an external gas inlet system, requires precursors with relatively large vapor pressures, about 10 Torr at operating temperature. This vapor pressure constraint is the reason all precursors used in hybrid MBE so far have been liquids. Unfortunately, in the case of the Pt-group metals, synthesizing a precursor with a suitably high vapor pressure for hybrid MBE has been difficult and no promising precursors have existed commercially. Instead, using solid metal–organics with a lower vapor pressure, although still orders of magnitude larger than the elemental metal, is an option. Generally, a vapor pressure between  $10^{-2}$  and  $10^{-5}$  Torr is desirable and is achievable with precursors like the Pt-group acetylacetonates at temperatures around 100 °C. In both cases, however, one must be careful of and operate below the decomposition temperatures. Additional advantages of precursors involve being able to form reactive radicals like with HMDT or containing oxygen like with TTIP for the growth of oxides.

## Growth rate

In the context of commercial production, growth rate is one of the most important figures of merit to compare different growth techniques. In MBE, increasing material complexity generally scales with lower growth rates. For example, growth rates of 20  $\mu\text{m/h}$  have been achieved in silicon MBE [138], and rates of 1  $\mu\text{m/h}$  have been achieved for MBE growth of binary compounds such as III–V semiconductors, III-nitride semiconductors, and  $\beta\text{-Ga}_2\text{O}_3$  [139–141]. However, growth rates within complex oxide MBE are typically less than 100 nm/h. Such slow rates are a major deterrent for the use of conventional oxide MBE in commercial production. Attempts have been made to overcome this issue with varying degrees of success. The main challenge associated with high growth rates in conventional oxide MBE has been non-stoichiometry-related defects forming after increasing the fluxes of the individual species.  $\text{SrTiO}_3$  is a good example of this; the high level of oxygen background pressure needed to increase the growth rate has caused source oxidation and resulting non-stoichiometry.

It was not until the development of hybrid MBE that growth rates of several hundred of nanometers per hour were achieved for complex oxides. By avoiding Ti source oxidation and supporting a growth window by supplying Ti as a gaseous precursor (TTIP), stoichiometric  $\text{SrTiO}_3$  films have been grown with rates exceeding 600 nm/h [142]. With TTIP contributing to the oxygen supply, large oxygen background pressures were not required to increase the growth rate. In fact, the reported growth rates were limited by the size of the Sr source and are predicted to approach 9  $\mu\text{m/h}$  if industrial size Sr sources are used [142].

## Outlook

We have discussed the evolution of MBE from the growth of III–V semiconductors to complex oxides for next-generation electronics. As new challenges have arisen, modifications have been made to the conventional approach to overcome them. Figure 6 summarizes the large number of source possibilities that have been developed. Due to MBE being a co-deposition or shuttered approach, the ability to mix and match these sources has made this technique extremely flexible and one of the top tools of choice for studying new materials.

An example of a material whose growth and study has seen rapid progress due, in large part, to MBE is  $\text{BaSnO}_3$ . This progress can be summarized by their mobilities plotted in Fig. 7a [12] which includes samples from PLD [20, 143–145], sputtering [114], MBE [60, 61, 113], and single crystals [21, 146–148]. Two main MBE variations have been used to grow  $\text{BaSnO}_3$ : supplying pre-oxidized Sn via  $\text{SnO}_2$  [60, 113, 123] and using the radical-based hybrid MBE approach to take advantage of the volatility and reactivity of the Sn-based radical components [61, 106, 108].

Both of these methods have achieved adsorption-controlled growth [60, 108]. The adoption of MBE to grow these materials has resulted in rapid improvement of the mobility from 70  $\text{cm}^2\text{V}^{-1}\text{s}^{-1}$  grown using PLD to 183  $\text{cm}^2\text{V}^{-1}\text{s}^{-2}$  grown using MBE [20, 60]. But the work of MBE in  $\text{BaSnO}_3$  thin films is not yet finished because despite these improvements, thin film mobilities still fall short of the 320  $\text{cm}^2\text{V}^{-1}\text{s}^{-1}$  demonstrated in single crystals [146]. One of the key reasons for this disparity is threading dislocations which form due to the lattice mismatch between  $\text{BaSnO}_3$  and all commercially available perovskite oxide substrates.  $\text{BaSnO}_3$  is a cubic perovskite with an exceptionally large lattice parameter of 4.116 Å and even the best-matched commercially available substrate  $\text{PrScO}_3$  (110) results in a -2.3% lattice mismatch [113, 149]. Other issues may also play detrimental roles on the mobility. These include imperfect stoichiometry, anti-site defects, and extrinsic impurities, all of which can compensate charge carriers and act as scattering centers.

Efforts are being made to address these problems and improve the electron mobility of  $\text{BaSnO}_3$ . New techniques to decrease threading dislocation density are being developed for the growth of bulk single crystals with lattice parameters closer to  $\text{BaSnO}_3$  [150, 151] and for high-quality lattice-matched films which can serve as “virtual” substrates [143]. Similarly, the buffer layer approach involves inserting an insulating layer of  $\text{BaSnO}_3$  or  $\text{Sr}_x\text{Ba}_{1-x}\text{SnO}_3$  between the substrate and doped “active” layer for the purpose of terminating threading dislocation propagation into the active layer [60, 61, 145]. Post-growth high-temperature annealing has been shown to eradicate some dislocations and other defects [152, 153]. Finally, early attempts at p-type doping of  $\text{BaSnO}_3$  have shown limited success, but there is much more required work to understand, improve, and exploit this phenomenon [154, 155].

Like  $\text{BaSnO}_3$ ,  $\text{SrSnO}_3$  is a wide bandgap alkaline-earth stannate semiconductor with a low electron effective mass. Whereas its smaller lattice parameter [107, 127, 156] may address some of the issues holding back  $\text{BaSnO}_3$ , its non-cubic perovskite structure and ultra-wide bandgap present additional challenges to its synthesis and doping, as well as opportunities for its performance in power electronics. Unlike  $\text{BaSnO}_3$ , however, there are no single-crystal studies of  $\text{SrSnO}_3$ . This makes thin film studies, at present, the only open experimental avenue to understand the fundamental transport properties of this exciting new material.  $\text{SrSnO}_3$  has been grown by PLD [157–165] and MBE [107, 123, 125–127, 166]. MBE studies include the use of the pre-oxidized  $\text{SnO}_2$  source [123] and the radical-based use of HMDT [107, 125–127, 166]. Interestingly, among films grown by MBE, only those using HMDT have reported successful doping. The use of HMDT has resulted in electron mobilities as high as 72  $\text{cm}^2\text{V}^{-1}\text{s}^{-1}$  [126]. Figure 7b shows the electron mobilities for MBE-grown  $\text{SrSnO}_3$  films [125, 166] and compares these values to those for some other UWBG semiconductors, which

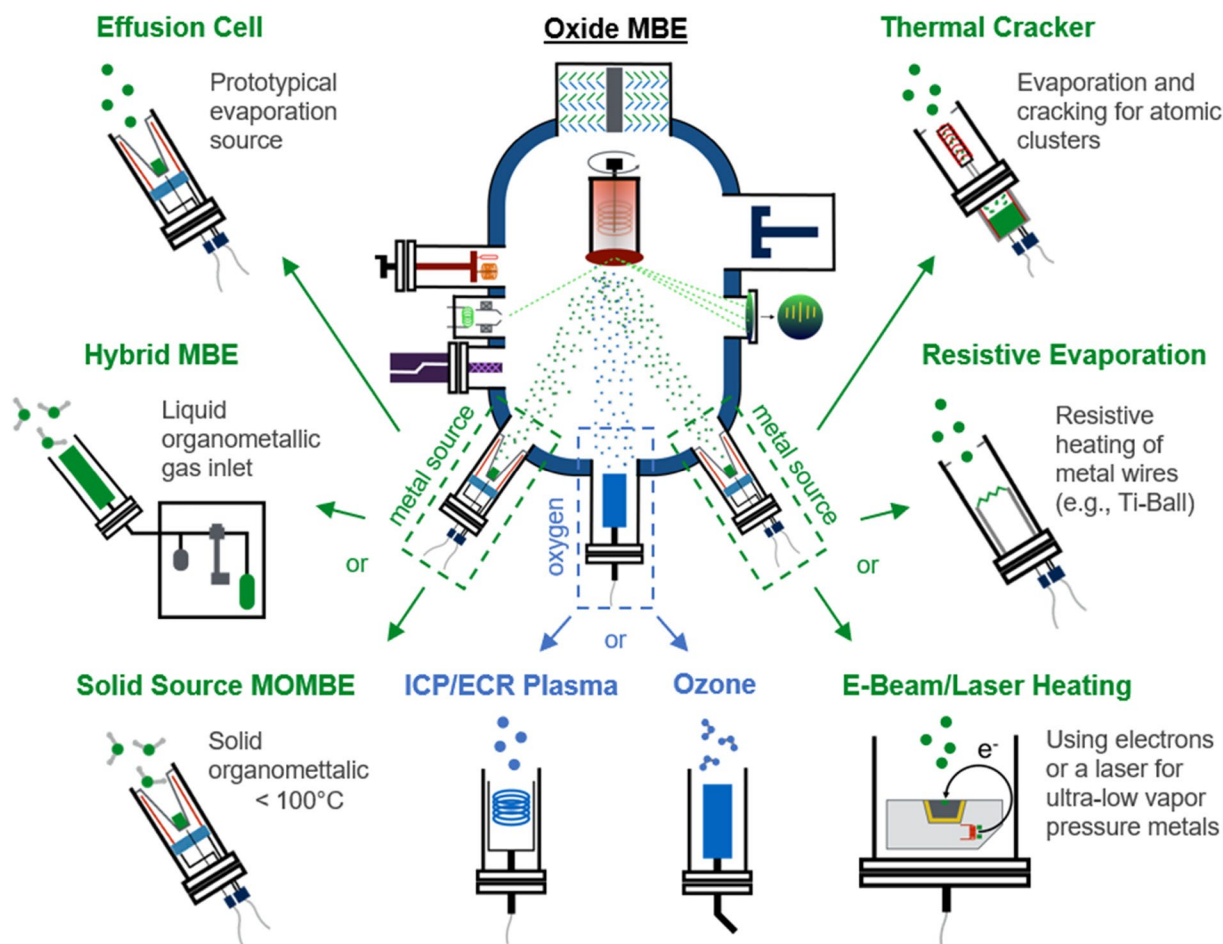


**Figure 6:** Schematic of the various common methods of delivering metal sources and oxidants in oxide MBE. Interchanging between sources has led MBE to become a very flexible technique.

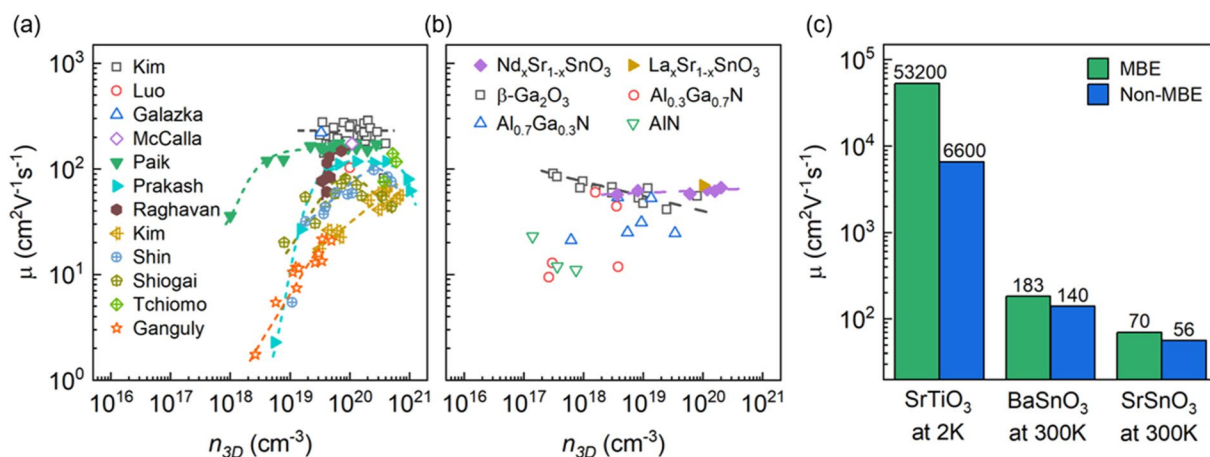


**Figure 7:** (a) Room-temperature electron mobility of BaSnO<sub>3</sub> single crystals (open symbol) [21, 146–148], MBE films (filled symbol) [60, 61, 113], PLD films (crossed symbols) [20, 143–145], and sputtered films (star) [114]. (b) Room-temperature electron mobility for SrSnO<sub>3</sub> MBE-grown films [125, 166] and other leading UWBG semiconductors [167–173]. (c) Record electron mobility for MBE and non-MBE films of SrTiO<sub>3</sub> at 2 K [100, 101], BaSnO<sub>3</sub> at 300 K [60, 143], and SrSnO<sub>3</sub> at 300 K [125, 165]. (a) [12] and (b) [166] adapted with permission.

is defined as those with a bandgap exceeding 4 eV [167–173]. As shown, the mobilities of SrSnO<sub>3</sub> exceed those of any other UWBG semiconductor at high carrier concentrations, an astounding result given SrSnO<sub>3</sub> research is still in its infancy. Hybrid MBE has been used to produce many electronic devices out of these materials including iongel-gated field-effect transistors [174], MOSFETs [175], MESFETs [176, 177], and RF FETs with the highest frequency operation of any complex oxide [178].

We conclude by discussing wide bandgap complex oxides most of which have not yet been grown by MBE, but might be of interest to pursue. Table 2 summarizes these compounds, their opportunities, and the challenges to MBE growth. Like SrTiO<sub>3</sub>, KTaO<sub>3</sub> is a quantum paraelectric with low-temperature mobilities as high as 23,000 cm<sup>2</sup>V<sup>-1</sup> s<sup>-1</sup> in single crystals [179]. It has gained recent attention due to the discovery of superconductivity induced by ionic gating [180] or at the interface with other oxides [181]. However, more than 50 years after the discovery of quantum paraelectricity in this compound, the lack of any MBE growth studies is surprising. This is a testament to the perceived challenges that the compound presents to MBE growers. K is a high-vapor pressure metal that is extremely prone to source oxidation, whereas Ta is a refractory metal with extremely low vapor pressure. However, both elements have been successfully supplied in oxide MBE [91, 182], so the challenge should not be regarded as insurmountable. Hybrid MBE is under development for Ta-containing complex oxides which may address some of these challenges [183].

The UWBG semiconductor CaSnO<sub>3</sub> shares many properties with SrSnO<sub>3</sub> but has a higher gap of ~4.4 eV making it very attractive for high-power electronics. However, the recent failed doping attempt using PLD raises the question of

whether the culprit is a material intrinsically unamenable to doping, some extrinsic effect such as point defects from high particle energies, or an inappropriate choice in dopant concentration [164]. Certainly, the higher bandgap in CaSnO<sub>3</sub> makes it more susceptible to intrinsic point defects which may self-compensate donors [184]. However, there are many extrinsic mechanisms that should be ruled out before denouncing the material itself. For example, PLD generates high-energy particles that can introduce point defects into the material which can act as acceptors that compensate the intentional donors. As a low-energy technique, MBE is a natural choice to rule out this possibility. Another area worth exploring is the use of alternative donors. La was chosen, which may seem like a natural choice given its success in doping BaSnO<sub>3</sub> and SrSnO<sub>3</sub> [107, 146]. However, Ca<sup>2+</sup> (1.48 Å) has a much smaller radius than Sr<sup>2+</sup> (1.58 Å) and Ba<sup>2+</sup> (1.75 Å), so smaller rare earth elements may be more appropriate for doping CaSnO<sub>3</sub>, B-site candidates such as V and Nb, and X-site candidates such as F are also worth exploring. Finally, the doping concentration chosen for this study was 4.9 × 10<sup>20</sup> cm<sup>-3</sup>. This donor concentration was found to be near optimal for SrSnO<sub>3</sub> [165], but is probably too high for CaSnO<sub>3</sub> given the doping limits can decrease with increasing bandgap.

Another class of UWBG semiconductors, (Mg,Zn)Ga<sub>2</sub>O<sub>4</sub>, are also promising. The cubic spinel ZnGa<sub>2</sub>O<sub>4</sub> has an indirect bandgap of 4.0–4.3 eV [185–187]. Electron mobilities as high as 107 cm<sup>2</sup>V<sup>-1</sup> s<sup>-1</sup> have been demonstrated in oxygen vacancy-doped single crystals [187]. MgGa<sub>2</sub>O<sub>4</sub> is a reverse spinel n-type semiconductor with a direct gap of 4.9 eV, but high mobilities have not been demonstrated [188, 189]. However, as with all spinel compounds, these compounds are very prone to anti-site defect formation, which can impede attempts to understand

**TABLE 2:** Promising wide and ultra-wide bandgap complex oxides and the challenges for their MBE deposition.

Material	Bandgap	Opportunity	Challenges	References
KTaO <sub>3</sub> , KNbO <sub>3</sub>	3.64 eV 3.24 eV	KTaO <sub>3</sub> is a high-mobility quantum paraelectric (like SrTiO <sub>3</sub> ). Ionic gating or 2DEG-induced superconductivity	K source oxidation, Ta and Nb low vapor pressure. Ta and Nb difficult to oxidize to 5+	[179–181, 201, 202]
CaSnO <sub>3</sub>	4.4 eV	Similar properties as SrSnO <sub>3</sub> , but with a wider bandgap	Previous failed doping attempts	[22, 164]
MgGa <sub>2</sub> O <sub>4</sub> , ZnGa <sub>2</sub> O <sub>4</sub>	4.9 eV, 4.0–4.3 eV	UWBG semiconductors with reverse and normal spinel structure, respectively	Anti-site defects	[187, 188, 190, 203]
(Ca,Sr,Ba)(Hf,Zr)O <sub>3</sub>	~ 5 to 6 eV	Doping case study for UWBG semiconductors Modulation donors Flat-band physics	Difficult to dope due to high bandgap and flat bands	[191–193, 204]
NaSbO <sub>3</sub>	3.4 eV	Direct wide bandgap semiconductor for optoelectronics	Sb tetramers. Oxidation to Sb <sup>5+</sup> difficult. Na prone to source oxidation. Metastable polymorph	[198]
CuMO <sub>2</sub> M = B, Al, Ga, In, Sc, Cr	~ 3.5 to 4.5 eV	p-type wide bandgap semiconductors	Oxidation of Cu. Suitable substrate selection	[199, 200]

their properties and sabotage device performance [190]. The precise stoichiometry control and low particle energy of MBE may be very helpful to fully understand and exploit the properties of these materials in devices.

Another group of materials with the perovskite oxide structure are the alkaline-earth zirconates and hafnates (Ca,Sr,Ba) (Zr,Hf)O<sub>3</sub>. These materials have been grown using MBE, but have generally been regarded as insulators because of their flat bands and gaps of over 5 eV in most cases. As a result, the literature is lacking in reports of doping attempts [191–193]. However, the appeal of electron doping these materials is three-fold. Firstly, they would serve as an excellent test to the limits of electron doping in oxides and are thus of strong interest to the growing field of UWBG semiconductors. Secondly, doping these materials would provide a new flat-band system to serve as an analog to SrTiO<sub>3</sub> and KTaO<sub>3</sub>, potentially hosting exotic transport phenomena. Finally, the high conduction band offset between these materials and more traditional complex oxide semiconductors make these compounds excellent candidates as donors in modulation-doped structures, [194] potentially enabling new high-mobility modulation-doped heterostructures. Liquid precursors have been developed for MBE and used for the growth of ZrO<sub>2</sub> [195], HfO<sub>2</sub> [196], and SrTi<sub>1-x</sub>Zr<sub>x</sub>O<sub>3</sub> [197], but we think there is much opportunity to capitalize on these early results.

NaSbO<sub>3</sub> is a metastable orthorhombic perovskite with a direct bandgap of 3.4 eV [198]. Analogous to BaSnO<sub>3</sub>, its conduction band is predominantly derived from Sb 5 s-orbitals which gives it a high level of dispersion and low electron effective mass. NaSbO<sub>3</sub> might provide high room-temperature electron mobilities as similarly found in BaSnO<sub>3</sub>. Whereas BaSnO<sub>3</sub> has an indirect bandgap, NaSbO<sub>3</sub> has a direct bandgap making it potentially useful for optoelectronic devices such as ultraviolet LEDs and visible-blind photodetectors. Whereas Na is an air-sensitive element highly prone to source oxidation, Sb evaporates as tetramers and is exceptionally difficult to oxidize to Sb<sup>5+</sup>. Finally, although structurally metastable perovskite polymorphs have been grown by oxide MBE [134], the associated growth challenges add an additional layer of difficulty to the process.

Finally, an interesting group of materials has emerged as possible p-type wide bandgap semiconductors in CuMO<sub>2</sub> with the delafossite structure where M = B, Al, Ga, In, Sc, or Cr. Stabilizing a p-type oxide with a wide bandgap would be highly advantageous for a myriad of devices [199] but these materials are problematic in MBE synthesis due to Cu oxidation and finding a suitable substrate for epitaxial growth. That said, MBE growth has been demonstrated. [200] However, stabilizing and studying all of these materials within this group is still underway.

Demonstrating the growth of these materials by MBE will require overcoming many of the challenges we have reviewed here: source oxidation, low oxidation potentials, ultra-low vapor pressures, and stoichiometry control. However, as can be seen by the record properties for many of these complex oxides (Fig. 7c), MBE is capable of growing some of the near perfect films currently available. By employing the multitude of MBE modifications that now exist, it is only a matter of time before these new wide bandgap complex oxides are reproducibly grown and applied in next-generation electronic and optoelectronic devices.

## Acknowledgments

The authors thank Scott Chambers for helpful discussion and proof-reading. We also thank Justin Ramberger and Javier Garcia Barriocanal for their helpful discussion regarding electron-beam evaporation and ozone MBE, respectively. This review paper acknowledges support from the Air Force Office of Scientific Research (AFOSR) through Grant Nos. FA9550-19-1-0245 and FA9550-21-1-0025 and through NSF DMR-1741801. We also acknowledge support from the U.S. Department of Energy through DE-SC002021 and the University of Minnesota Center for Quantum Materials, under Award No. DE-SC0016371. The work also benefitted from the Norwegian Centennial Chair Program (NOCC) and Vannevar Bush Faculty Fellowship and the UMN MRSEC program under Award No. DMR-2011401. W.N. thanks support from the UMN doctoral dissertation fellowship.

## Data availability

Data sharing is not applicable to this article as this is review article and that there were no new datasets generated or analyzed.

## Declarations

**Conflict of interest** There is no conflict of interest.

## References

1. J. Shi, J. Zhang, L. Yang, M. Qu, D.C. Qi, K.H. Zhang, Wide bandgap oxide semiconductors: from materials physics to optoelectronic devices. *Adv. Mater.* 2006230 (2021).
2. J. Robertson, Band offsets of wide-band-gap oxides and implications for future electronic devices. *J. Vac. Sci. Technol. B* 18(3), 1785 (2000)
3. S. Fujita, Wide-bandgap semiconductor materials: for their full bloom. *Jpn. J. Appl. Phys.* 54(3), 030101 (2015)

4. S. Jin, T.H. Tiefel, M. McCormack, R.A. Fastnacht, R. Ramesh, L.H. Chen, Thousandfold change in resistivity in magnetoresistive La-Ca-Mn-O films. *Science* **264**(5157), 413 (1994)
5. J.G. Bednorz, K.A. Müller, Possible high  $T_c$  superconductivity in the Ba-La-Cu-O system. *Z. Phys. B.* **64**(2), 189 (1986)
6. S. Pei, J.D. Jorgensen, D.G. Hinks, P. Lightfoot, Y. Zheng, D.R. Richards, B. Dabrowski, A.W. Mitchell, Structure of  $BaBiO_{3-\delta}$  at high temperature. *Mater. Res. Bull.* **25**(12), 1467 (1990)
7. G.A. Smolenskii, I.E. Chupis, Ferroelectromagnets. *Soviet Physics Uspekhi.* **25**(7), 475 (1982)
8. Y. Shi, Y. Guo, X. Wang, A.J. Princep, D. Khalayin, P. Manuel, Y. Michiue, A. Sato, K. Tsuda, S. Yu, M. Arai, Y. Shirako, M. Akaogi, N. Wang, K. Yamaura, A.T. Boothroyd, A ferroelectric-like structural transition in a metal. *Nat. Mater.* **12**(11), 1024 (2013)
9. F. Baiutti, G. Christiani, G. Logvenov, Towards precise defect control in layered oxide structures by using oxide molecular beam epitaxy. *Beilstein J. Nanotechnol.* **5**(1), 596 (2014)
10. D.G. Schlom, Perspective: oxide molecular-beam epitaxy rocks! *APL Mater.* **3**(6), 062403 (2015).
11. M. Brahlek, A.S. Gupta, J. Lapano, J. Roth, H.T. Zhang, L. Zhang, R. Haislmaier, R. Engel-Herbert, Frontiers in the growth of complex oxide thin films: past, present, and future of hybrid MBE. *Adv. Funct. Mater.* **28**(9), 1702772 (2018)
12. A. Prakash, B. Jalan, Wide bandgap perovskite oxides with high room-temperature electron mobility. *Adv. Mater. Interfaces.* **6**(15), 1900479 (2019)
13. J. MacManus-Driscoll, M.P. Wells, C. Yun, J.-W. Lee, C.-B. Eom, D.G. Schlom, New approaches for achieving more perfect transition metal oxide thin films. *APL Mater.* **8**(4), 040904 (2020)
14. J.H.N. Divine, P. Kumah, L. Kornblum, Epitaxial oxides on semiconductors: from fundamentals to new devices. *Adv. Funct. Mater.* **30**, 1901597 (2020)
15. S.A. Chambers, T.C. Kaspar, A. Prakash, G. Haugstad, B. Jalan, Band alignment at epitaxial  $BaSnO_3/SrTiO_3$  (001) and  $BaSnO_3/LaAlO_3$  (001) heterojunctions. *Appl. Phys. Lett.* **108**(15), 152104 (2016)
16. O. Tufte, P. Chapman, Electron mobility in semiconducting strontium titanate. *Phys. Rev.* **155**(3), 796 (1967)
17. J.F. Schooley, W.R. Hosler, M.L. Cohen, Superconductivity in semiconducting  $SrTiO_3$ . *Phys. Rev. Lett.* **12**(17), 474 (1964)
18. A. Ohtomo, H.Y. Hwang, A high-mobility electron gas at the  $LaAlO_3/SrTiO_3$  heterointerface. *Nature* **427**(6973), 423 (2004)
19. M.C. Tarun, F.A. Selim, M.D. McCluskey, Persistent photoconductivity in strontium titanate. *Phys. Rev. Lett.* **111**(18), 187403 (2013)
20. H.J. Kim, U. Kim, H.M. Kim, T.H. Kim, H.S. Mun, B.-G. Jeon, K.T. Hong, W.-J. Lee, C. Ju, K.H. Kim, K. Char, High mobility in a stable transparent perovskite oxide. *Appl. Phys. Express.* **5**(6), 061102 (2012)
21. X. Luo, Y.S. Oh, A. Sirenko, P. Gao, T. Tyson, K. Char, S.-W. Cheong, High carrier mobility in transparent  $Ba_{1-x}La_xSnO_3$  crystals with a wide band gap. *Appl. Phys. Lett.* **100**(17), 172112 (2012)
22. H. Mizoguchi, H.W. Eng, P.M. Woodward, Probing the electronic structures of ternary perovskite and pyrochlore oxides containing  $Sn^{4+}$  or  $Sb^{5+}$ . *Inorg. Chem.* **43**(5), 1667 (2004)
23. T. Stanislavchuk, A. Sirenko, A. Litvinchuk, X. Luo and S.-W. Cheong, Electronic band structure and optical phonons of  $BaSnO_3$  and  $Ba_{0.97}La_{0.03}SnO_3$  single crystals: theory and experiment. *J. Appl. Phys.* **112**(4), 044108 (2012).
24. C.A. Niedermeier, S. Rhode, K. Ide, H. Hiramatsu, H. Hosono, T. Kamiya, M.A. Moram, Electron effective mass and mobility limits in degenerate perovskite stannate  $BaSnO_3$ . *Phys. Rev. B.* **95**(16), 161202 (2017)
25. S.J. Allen, S. Raghavan, T. Schumann, K.-M. Law, S. Stemmer, Conduction band edge effective mass of La-doped  $BaSnO_3$ . *Appl. Phys. Lett.* **108**(25), 252107 (2016)
26. K. Krishnaswamy, B. Himmetoglu, Y. Kang, A. Janotti, C.G. Van de Walle, First-principles analysis of electron transport in  $BaSnO_3$ . *Phys. Rev. B.* **95**(20), 205202 (2017)
27. J.E. Greene, Tracing the recorded history of thin-film sputter deposition: from the 1800s to 2017. *J. Vac. Sci. Technol. A.* **35**(5), 05C204 (2017)
28. W.R. Grove, On the electro-chemical polarity of gases. *Philos. Trans. R. Soc. Lond.* (142), 87 (1852).
29. M. Faraday, Experimental relations of gold (and other metals) to light. *Philos. Trans. R. Soc. Lond.* (147), 145 (1857).
30. H.M. Smith, A. Turner, Vacuum deposited thin films using a ruby laser. *Appl. Opt.* **4**(1), 147 (1965)
31. P. Ganguly, C. Rao, Crystal chemistry and magnetic properties of layered metal oxides possessing the  $K_2NiF_4$  or related structures. *J. Solid State Chem.* **53**(2), 193 (1984)
32. D. Dijkkamp, T. Venkatesan, X. Wu, S. Shaheen, N. Jisrawi, Y. Min-Lee, W. McLean, M. Croft, Preparation of Y-Ba-Cu oxide superconductor thin films using pulsed laser evaporation from high  $T_c$  bulk material. *Appl. Phys. Lett.* **51**(8), 619 (1987)
33. M.-K. Wu, J.R. Ashburn, C. Torng, P.H. Hor, R.L. Meng, L. Gao, Z.J. Huang, Y. Wang, A. Chu, Superconductivity at 93 K in a new mixed-phase Y-Ba-Cu-O compound system at ambient pressure. *Phys. Rev. Lett.* **58**(9), 908 (1987)
34. J.R. Arthur, Interaction of Ga and  $As_2$  molecular beams with GaAs surfaces. *J. Appl. Phys.* **39**(8), 4032 (1968)
35. A.Y. Cho, J.R. Arthur, Molecular beam epitaxy. *Prog. Solid. State Ch.* **10**, 157 (1975)
36. W.P. McCray, MBE deserves a place in the history books. *Nat. Nanotechnol.* **2**(5), 259 (2007)
37. P.F. Michel: Coating by cathode disintegration. 2,146,025 (7 Feb. 1939).

38. B. Jalan, R. Engel-Herbert, N.J. Wright, S. Stemmer, Growth of high-quality SrTiO<sub>3</sub> films using a hybrid molecular beam epitaxy approach. *J. Vac. Sci. Technol. A.* **27**(3), 461 (2009)
39. W. Nunn, A.K. Manjeshwar, J. Yue, A. Rajapitamahuni, T.K. Truttman, B. Jalan, Novel synthesis approach for “Stub-born” metals and metal oxides. *Proc. Natl. Acad. Sci.* **118**(32), e2105713118 (2021)
40. C.-B. Eom, J. Lee, Metal-organic pulsed laser deposition for stoichiometric complex oxide thin films. (6 Oct. 2020).
41. R. Dingle, H. Störmer, A. Gossard, W. Wiegmann, Electron mobilities in modulation-doped semiconductor heterojunction superlattices. *Appl. Phys. Lett.* **33**(7), 665 (1978)
42. H.L. Stormer, Nobel lecture: the fractional quantum Hall effect. *Rev. Mod. Phys.* **71**(4), 875 (1999)
43. D.L. Smith, V.Y. Pickhardt, Molecular beam epitaxy of II-VI compounds. *J. Appl. Phys.* **46**(6), 2366 (1975)
44. S. Yoshida, S. Misawa, Y. Fujii, S. Takada, H. Hayakawa, S. Gonda, A. Itoh, Reactive molecular beam epitaxy of aluminium nitride. *J. Vac. Sci. Technol.* **16**(4), 990 (1979)
45. A. Koma, K. Sunouchi, T. Miyajima, Fabrication and characterization of heterostructures with subnanometer thickness. *Microelectron. Eng.* **2**(1–3), 129 (1984)
46. R. Betts, C. Pitt, Growth of thin-film lithium niobate by molecular beam epitaxy. *Electron. Lett.* **21**(21), 960 (1985)
47. J. Kwo, T. Hsieh, R. Fleming, M. Hong, S.H. Liou, B. Davidson, Feldman and LC: structural and superconducting properties of orientation-ordered Y<sub>1</sub>Ba<sub>2</sub>Cu<sub>3</sub>O<sub>7-x</sub> films prepared by molecular-beam epitaxy. *Phys. Rev. B.* **36**(7), 4039 (1987)
48. C. Webb, S.L. Weng, J. Eckstein, N. Missert, K. Char, D. Schlom, E. Hellman, M. Beasley, A. Kapitulnik, J. Harris Jr., Growth of high T<sub>c</sub> superconducting thin films using molecular beam epitaxy techniques. *Appl. Phys. Lett.* **51**(15), 1191 (1987)
49. D.D. Berkley, B.R. Johnson, N. Anand, K.M. Beauchamp, L.E. Conroy, A.M. Goldman, J. Maps, K. Mauersberger, M.L. Mecartney, J. Morton, M. Tuominen, Y.J. Zhang, In situ formation of superconducting YBa<sub>2</sub>Cu<sub>3</sub>O<sub>7-x</sub> thin films using pure ozone vapor oxidation. *Appl. Phys. Lett.* **53**(20), 1973 (1988)
50. D.G. Schlom, A. Marshall, J. Sizemore, Z. Chen, J. Eckstein, I. Bozovic, K. Von Dessionneck, J. Harris Jr., J. Bravman, Molecular beam epitaxial growth of layered Bi-Sr-Ca-Cu-O compounds. *J. Cryst. Growth.* **102**(3), 361 (1990)
51. Y. Segawa, A. Ohtomo, M. Kawasaki, H. Koinuma, Z. Tang, P. Yu, G. Wong, Growth of ZnO thin film by laser MBE: lasing of exciton at room temperature. *Phys. Status Solidi B.* **202**(2), 669 (1997)
52. M. Johnson, S. Fujita, W. Rowland, W. Hughes, J. Cook, J. Schetzina, MBE growth and properties of ZnO on sapphire and SiC substrates. *J. Electron. Mater.* **25**(5), 855 (1996)
53. J. Falson, Y. Kozuka, M. Uchida, J.H. Smet, T.-H. Arima, A. Tsukazaki, M. Kawasaki, MgZnO/ZnO heterostructures with electron mobility exceeding 1×10<sup>6</sup> cm<sup>2</sup>/Vs. *Sci. Rep.* **6**(1), 1 (2016)
54. S. Migita, Y. Kasai, H. Ota, S. Sakai, Self-limiting process for the bismuth content in molecular beam epitaxial growth of Bi<sub>2</sub>Sr<sub>2</sub>CuO<sub>y</sub> thin films. *Appl. Phys. Lett.* **71**(25), 3712 (1997)
55. C.D. Theis, J. Yeh, D.G. Schlom, M. Hawley, G. Brown, Adsorption-controlled growth of PbTiO<sub>3</sub> by reactive molecular beam epitaxy. *Thin Solid Films* **325**(1–2), 107 (1998)
56. C.D. Theis, J. Yeh, D.G. Schlom, M. Hawley, G. Brown, J. Jiang, X. Pan, Adsorption-controlled growth of Bi<sub>4</sub>Ti<sub>3</sub>O<sub>12</sub> by reactive MBE. *Appl. Phys. Lett.* **72**(22), 2817 (1998)
57. G. Zhang, H. Qin, J. Teng, J. Guo, Q. Guo, X. Dai, Z. Fang, K. Wu, Quintuple-layer epitaxy of thin films of topological insulator Bi<sub>2</sub>Se<sub>3</sub>. *Appl. Phys. Lett.* **95**(5), 053114 (2009)
58. A. Mellnik, J. Lee, A. Richardella, J. Grab, P. Mintun, M.H. Fischer, A. Vaezi, A. Manchon, E.-A. Kim, N. Samarth, Spin-transfer torque generated by a topological insulator. *Nature* **511**(7510), 449 (2014)
59. J.A. Mundy, C.M. Brooks, M.E. Holtz, J.A. Moyer, H. Das, A.F. Rébola, J.T. Heron, J.D. Clarkson, S.M. Disseler, Z. Liu, Atomically engineered ferroic layers yield a room-temperature magnetoelectric multiferroic. *Nature* **537**(7621), 523 (2016)
60. H. Paik, Z. Chen, E. Lochocki, A. Seidner, A. Verma, N. Tanen, J. Park, M. Uchida, S. Shang, B.-C. Zhou, M. Brützmam, R. Uecker, Z.-K. Liu, J. Debdeep, K.M. Shen, D.A. Muller, D.G. Schlom, Adsorption-controlled growth of La-doped BaSnO<sub>3</sub> by molecular-beam epitaxy. *APL Mater.* **5**(11), 116107 (2017)
61. A. Prakash, P. Xu, A. Faghaninia, S. Shukla, J.W. Ager, C.S. Lo, B. Jalan, Wide bandgap BaSnO<sub>3</sub> films with room temperature conductivity exceeding 10<sup>4</sup> S cm<sup>-1</sup>. *Nat. Commun.* **8**(1), 1 (2017)
62. W. Li, J. Shi, K.H. Zhang, J.L. MacManus-Driscoll, Defects in complex oxide thin films for electronics and energy applications: challenges and opportunities. *Mater. Horiz.* **7**(11), 2832 (2020)
63. V. Matias, R.H. Hammond, Ion beam induced crystalline texturing during thin film deposition. *Surf. Coat. Technol.* **264**, 1 (2015)
64. T. Ohnishi, K. Shibuya, T. Yamamoto, M. Lippmaa, Defects and transport in complex oxide thin films. *J. Appl. Phys.* **103**(10), 103703 (2008)
65. D.M. Dobkin, M.K. Zaraw, Principles of Chemical Vapor Deposition (Springer, City, 2003).
66. J. Haeni, C. Theis, D. Schlom, W. Tian, X. Pan, H. Chang, I. Takeuchi, X.-D. Xiang, Epitaxial growth of the first five members of the Sr<sub>n+1</sub>Ti<sub>n</sub>O<sub>3n+1</sub> Ruddlesden-Popper homologous series. *Appl. Phys. Lett.* **78**(21), 3292 (2001)
67. W. Tian, J.H. Haeni, D.G. Schlom, E. Hutchinson, B.L. Sheu, M.M. Rosario, P. Schiffer, Y. Liu, M.A. Zurbuchen, X.Q. Pan, Epitaxial growth and magnetic properties of the first five

- members of the layered  $\text{Sr}_{n+1}\text{Ru}_n\text{O}_{3n+1}$  oxide series. *Appl. Phys. Lett.* **90**(2), 022507 (2007)
68. C.-H. Lee, N.D. Orloff, T. Birol, Y. Zhu, V. Goian, E. Rocas, R. Haislmaier, E. Vlahos, J.A. Mundy, L.F. Kourkoutis, Y. Nie, M.D. Biegalski, J. Zhang, M. Bernhagen, N.A. Benedek, Y. Kim, J.D. Brock, R. Uecker, X.X. Xi, V. Gopalan, D. Nuzhnyy, S. Kamba, D.A. Muller, I. Takeuchi, J.C. Booth, C.J. Fennie, D.G. Schlom, Exploiting dimensionality and defect mitigation to create tunable microwave dielectrics. *Nature* **502**(7472), 532 (2013)
  69. R.C. Haislmaier, G. Stone, N. Alem, R. Engel-Herbert, Creating Ruddlesden-Popper phases by hybrid molecular beam epitaxy. *Appl. Phys. Lett.* **109**(4), 043102 (2016)
  70. M.R. Barone, N.M. Dawley, H.P. Nair, B.H. Goodge, M.E. Holtz, A. Soukiasian, E.E. Fleck, K. Lee, Y. Jia, T. Heeg, R. Gatt, Y. Nie, D.A. Muller, L.F. Kourkoutis, D.G. Schlom, Improved control of atomic layering in perovskite-related homologous series. *APL Mater.* **9**(2), 021118 (2021)
  71. C.-H. Lee, N.J. Podraza, Y. Zhu, R.F. Berger, S. Shen, M. Sestak, R.W. Collins, L.F. Kourkoutis, J.A. Mundy, H. Wang, Q. Mao, X. Xi, L.J. Brillson, J.B. Neaton, D.A. Muller, D.G. Schlom, Effect of reduced dimensionality on the optical band gap of  $\text{SrTiO}_3$ . *Appl. Phys. Lett.* **102**(12), 122901 (2013)
  72. Y.F. Nie, Y. Zhu, C.H. Lee, L.F. Kourkoutis, J.A. Mundy, J. Junquera, P. Ghosez, D.J. Baek, S. Sung, X.X. Xi, K.M. Shen, D.A. Muller, D.G. Schlom, Atomically precise interfaces from non-stoichiometric deposition. *Nat. Commun.* **5**(1), 4530 (2014)
  73. U. Poppe, J. Schubert, R.R. Arons, W. Evers, C.H. Freiburg, W. Reichert, K. Schmidt, W. Sybertz, K. Urban, Direct production of crystalline superconducting thin films of  $\text{YBa}_2\text{Cu}_3\text{O}_7$  by high-pressure oxygen sputtering. *Solid State Commun.* **66**(6), 661 (1988)
  74. A. Guarino, G. Patimo, A. Vecchione, T. Di Luccio, A. Nigro, Fabrication of superconducting  $\text{Nd}_{2-x}\text{Ce}_x\text{CuO}_{4\pm\delta}$  films by automated DC sputtering technique. *Physica C* **495**, 146 (2013)
  75. M. Schmitz, A. Weber, O. Petravic, M. Waschke, P. Zakalek, S. Mattau, A. Koutsoubas, T. Brückel, Strain and electric field control of magnetism in  $\text{La}_{1-x}\text{Sr}_x\text{MnO}_3$  thin films on ferroelectric  $\text{BaTiO}_3$  substrates. *N. J. Phys.* **22**(5), 053018 (2020)
  76. J.R. Contreras, H. Kohlstedt, A. Petraru, A. Gerber, B. Hermanns, H. Haselier, N. Nagarajan, J. Schubert, U. Poppe, C. Buchal, R. Waser, Improved  $\text{PbZr}_{0.52}\text{Ti}_{0.48}\text{O}_3$  film quality on  $\text{SrRuO}_3/\text{SrTiO}_3$  substrates. *J. Cryst. Growth.* **277**(1), 210 (2005)
  77. P.C. Feijoo, M.A. Pampillón, E.S. Andrés, J.L.G. Fierro, Nanolaminate vs. direct deposition of high permittivity gadolinium scandate on silicon by high pressure sputtering. *Thin Solid Films* **593**, 62 (2015)
  78. A. Petraru, N.A. Pertsev, H. Kohlstedt, U. Poppe, R. Waser, A. Solbach, U. Klemradt, Polarization and lattice strains in epitaxial  $\text{BaTiO}_3$  films grown by high-pressure sputtering. *J. Appl. Phys.* **101**(11), 114106 (2007)
  79. P. Ambwani, P. Xu, G. Haugstad, J.S. Jeong, R. Deng, K.A. Mkhoyan, B. Jalan, C. Leighton, Defects, stoichiometry, and electronic transport in  $\text{SrTiO}_{3-\delta}$  epilayers: a high pressure oxygen sputter deposition study. *J. Appl. Phys.* **120**(5), 055704 (2016)
  80. K. Ganguly, P. Ambwani, P. Xu, J.S. Jeong, K.A. Mkhoyan, C. Leighton, B. Jalan, Structure and transport in high pressure oxygen sputter-deposited  $\text{BaSnO}_{3-\delta}$ . *APL Mater.* **3**, 062509 (2015)
  81. W.M. Postiglione, K. Ganguly, H. Yun, J.S. Jeong, A. Jacobson, L. Borgeson, B. Jalan, K.A. Mkhoyan, C. Leighton, Structure-property relationships and mobility optimization in sputtered La-doped  $\text{BaSnO}_3$  films: Toward  $100\text{ cm}^2\text{V}^{-1}\text{s}^{-1}$  mobility. *Phys. Rev. Mater.* **5**(4), 044604 (2021)
  82. R. Zhang, X. Li, J. Bi, S. Zhang, S. Peng, Y. Song, Q. Zhang, L. Gu, J. Duan, Y. Cao, One-step epitaxy of high-mobility La-doped  $\text{BaSnO}_3$  films by high-pressure magnetron sputtering. *APL Mater.* **9**(6), 061103 (2021)
  83. C.X. Zheng, K. Hannikainen, Y.R. Niu, J. Tersoff, D. Gomez, J. Pereiro, D.E. Jesson, Mapping the surface phase diagram of  $\text{GaAs}(001)$  using droplet epitaxy. *Phys. Rev. Mater.* **3**(12), 124603 (2019)
  84. S.A. Chambers, Epitaxial growth and properties of thin film oxides. *Surf. Sci. Rep.* **39**(5–6), 105 (2000)
  85. S. Thapa, R. Paudel, M.D. Blanchet, P.T. Gemperline, R.B. Comes, Probing surfaces and interfaces in complex oxide films via in situ X-ray photoelectron spectroscopy. *J. Mater. Res.* **36**, 26 (2021)
  86. T. Orvis, T. Cao, M. Surendran, H. Kumarasubramanian, A.S. Thind, A. Cunniff, R. Mishra, J. Ravichandran, Direct observation and control of surface termination in perovskite oxide heterostructures. *Nano Lett.* **21**(10), 4160 (2021)
  87. T. Orvis, H. Kumarasubramanian, M. Surendran, S. Kutagulla, A. Cunniff, J. Ravichandran, In situ monitoring of composition and sensitivity to growth parameters of pulsed laser deposition. *ACS Appl. Electron. Mater.* **3**(3), 1422 (2021)
  88. Y. Watanabe, Y.F. Nishimura, R. Suzuki, H. Uehara, T. Nimura, A. Beniya, N. Isomura, K. Asakura, S. Takakusagi, Portable ultrahigh-vacuum sample storage system for polarization-dependent total-reflection fluorescence x-ray absorption fine structure spectroscopy. *J. Vac. Sci. Technol. A.* **34**(2), 023201 (2015)
  89. M. Klausmeier-Brown, J. Eckstein, I. Bozovic, G. Virshup, Accurate measurement of atomic beam flux by pseudo-double-beam atomic absorption spectroscopy for growth of thin-film oxide superconductors. *Appl. Phys. Lett.* **60**(5), 657 (1992)
  90. C. Lu, M.J. Lightner, C.A. Gogol, Rate controlling and composition analysis of alloy deposition processes by electron impact emission spectroscopy (EIES). *J. Vac. Sci. Technol.* **14**(1), 103 (1977)

91. H. Yamamoto, K. Aoki, A. Tsukada, M. Naito, Growth of  $Ba_{1-x}K_xBiO_3$  thin films by molecular beam epitaxy. *Physica C* **412–414**, 192 (2004)
92. C. Lu, C.D. Blissett, G. Diehl, An electron impact emission spectroscopy flux sensor for monitoring deposition rate at high background gas pressure with improved accuracy. *J. Vac. Sci. Technol. A.* **26**(4), 956 (2008)
93. J. Haeni, C.D. Theis, D.G. Schlom, RHEED intensity oscillations for the stoichiometric growth of  $SrTiO_3$  thin films by reactive molecular beam epitaxy. *J. Electroceram.* **4**(2), 385 (2000)
94. D. Schlom, J. Haeni, J. Lettieri, C. Theis, W. Tian, J. Jiang, X. Pan, Oxide nano-engineering using MBE. *Mater. Sci. Eng. B.* **87**(3), 282 (2001)
95. R.A. Kubiak, S.M. Newstead, A.R. Powell, E.H.C. Parker, T.E. Whall, T. Naylor, K. Bowen, Improved flux control from the Sentinel III electron impact emission spectroscopy system. *J. Vac. Sci. Technol. A.* **9**(4), 2423 (1991)
96. C.D. Theis, D.G. Schlom, Epitaxial lead titanate grown by MBE. *J. Cryst. Growth.* **174**(1–4), 473 (1997)
97. B. Jalan, P. Moetakef, S. Stemmer, Molecular beam epitaxy of  $SrTiO_3$  with a growth window. *Appl. Phys. Lett.* **95**(3), 032906 (2009)
98. C.D. Theis, D.G. Schlom, Cheap and stable titanium source for use in oxide molecular beam epitaxy systems. *J. Vac. Sci. Technol. A.* **14**(4), 2677 (1996)
99. Y.S. Kim, N. Bansal, C. Chaparro, H. Gross, S. Oh, Sr flux stability against oxidation in oxide-molecular-beam-epitaxy environment: flux, geometry, and pressure dependence. *J. Vac. Sci. Technol. A.* **28**(2), 271 (2010)
100. T.A. Cain, A.P. Kajdos and S. Stemmer: La-doped  $SrTiO_3$  films with large cryogenic thermoelectric power factors. *Appl. Phys. Lett.* **102**(18), 182101 (2013).
101. Y. Kozuka, Y. Hikita, C. Bell, H. Hwang, Dramatic mobility enhancements in doped  $SrTiO_3$  thin films by defect management. *Appl. Phys. Lett.* **97**(1), 012107 (2010)
102. Y. Matsubara, K.S. Takahashi, Y. Tokura, M. Kawasaki, Single-crystalline  $BaTiO_3$  films grown by gas-source molecular beam epitaxy. *Appl. Phys. Express.* **7**(12), 125502 (2014)
103. P. Moetakef, J.Y. Zhang, S. Raghavan, A.P. Kajdos, S. Stemmer, Growth window and effect of substrate symmetry in hybrid molecular beam epitaxy of a Mott insulating rare earth titanate. *J. Vac. Sci. Technol. A.* **31**(4), 041503 (2013)
104. S. Raghavan, J.Y. Zhang, O.F. Shoron, S. Stemmer, Probing the metal-insulator transition in  $BaTiO_3$  by electrostatic doping. *Phys. Rev. Lett.* **117**(3), 037602 (2016)
105. J.A. Moyer, C. Eaton, R. Engel-Herbert, Highly conductive  $SrVO_3$  as a bottom electrode for functional perovskite oxides. *Adv. Mater.* **25**(26), 3578 (2013)
106. A. Prakash, J. Dewey, H. Yun, J.S. Jeong, K.A. Mkhoyan, B. Jalan, Hybrid molecular beam epitaxy for the growth of stoichiometric  $BaSnO_3$ . *J. Vac. Sci. Technol. A.* **33**(6), 060608 (2015)
107. T. Wang, L.R. Thoutam, A. Prakash, W. Nunn, G. Haugstad, B. Jalan, Defect-driven localization crossovers in MBE-grown La-doped  $SrSnO_3$  films. *Phys. Rev. Mater.* **1**(6), 061601 (2017)
108. A. Prakash, P. Xu, X. Wu, G. Haugstad, X. Wang, B. Jalan, Adsorption-controlled growth and the influence of stoichiometry on electronic transport in hybrid molecular beam epitaxy-grown  $BaSnO_3$  films. *J. Mater. Chem. C.* **5**(23), 5730 (2017)
109. W. Braun, M. Jäger, G. Laskin, P. Ngabonziza, W. Voesch, P. Witzlich, J. Mannhart, In situ thermal preparation of oxide surfaces. *APL Mater.* **8**(7), 071112 (2020)
110. J.R. Rumble, *CRC Handbook of Chemistry and Physics* (CRC Press, Boca Raton, 2020)
111. D.A. Muller, N. Nakagawa, A. Ohtomo, J.L. Grazul, H.Y. Hwang, Atomic-scale imaging of nanoengineered oxygen vacancy profiles in  $SrTiO_3$ . *Nature* **430**(7000), 657 (2004)
112. H. Yang, Y. Wang, H. Wang, Q. Jia, Oxygen concentration and its effect on the leakage current in  $BiFeO_3$  thin films. *Appl. Phys. Lett.* **96**(1), 012909 (2010)
113. S. Raghavan, T. Schumann, H. Kim, J.Y. Zhang, T.A. Cain, S. Stemmer, High-mobility  $BaSnO_3$  grown by oxide molecular beam epitaxy. *APL Mater.* **4**(1), 016106 (2016)
114. K. Ganguly, A. Prakash, B. Jalan, C. Leighton, Mobility-electron density relation probed via controlled oxygen vacancy doping in epitaxial  $BaSnO_3$ . *APL Mater.* **5**(5), 056102 (2017)
115. D.G. Schlom, J.S. Harris, MBE growth of high- $T_c$  superconductors, in molecular beam epitaxy - applications to key materials, edited by R. F. C. Farrow (Noyes, Park Ridge, City, 1995), pp. 505.
116. D. Schlom, J. Eckstein, E. Hellman, S. Streiffner, J. Harris Jr., M. Beasley, J. Bravman, T. Geballe, C. Webb, K. Von Dessenneck, F. Turner, Molecular beam epitaxy of layered Dy-Ba-Cu-O compounds. *Appl. Phys. Lett.* **53**(17), 1660 (1988)
117. J.P. Locquet, E. Mächler, Characterization of a radio frequency plasma source for molecular beam epitaxial growth of high- $T_c$  superconductor films. *J. Vac. Sci. Technol. A.* **10**(5), 3100 (1992)
118. Y. Gao, S.A. Chambers, Heteroepitaxial growth of  $\alpha$ - $Fe_2O_3$ ,  $\gamma$ - $Fe_2O_3$  and  $Fe_3O_4$  thin films by oxygen-plasma-assisted molecular beam epitaxy. *J. Cryst. Growth.* **174**(1–4), 446 (1997)
119. D. Lind, S. Berry, G. Chern, H. Mathias, L. Testardi, Growth and structural characterization of  $Fe_3O_4$  and NiO thin films and superlattices grown by oxygen-plasma-assisted molecular-beam epitaxy. *Phys. Rev. B.* **45**(4), 1838 (1992)
120. N. Materer, R.S. Goodman, S.R. Leone, Comparison of electron cyclotron resonance and radio-frequency inductively coupled plasmas of Ar and  $N_2$ : Neutral kinetic energies and source gas cracking. *J. Appl. Phys.* **83**(4), 1917 (1998)
121. K. Sakurai, D. Iwata, S. Fujita and S. Fujita, Growth of ZnO by molecular beam epitaxy using  $NO_2$  as oxygen source. *Jpn. J. Appl. Phys.* **38**(Part 1, No. 4B), 2606 (1999).

122. N. Izyumskaya, V. Avrutin, W. Schoch, A. El-Shaer, F. Reuß, T. Gruber, A. Waag, Molecular beam epitaxy of high-quality ZnO using hydrogen peroxide as an oxidant. *J. Cryst. Growth.* **269**(2), 356 (2004)
123. T. Schumann, S. Raghavan, K. Ahadi, H. Kim, S. Stemmer, Structure and optical band gaps of (Ba, Sr)SnO<sub>3</sub> films grown by molecular beam epitaxy. *J. Vac. Sci. Technol. A.* **34**(5), 050601 (2016)
124. L. Zhang, R. Engel-Herbert, Growth of SrTiO<sub>3</sub> on Si (001) by hybrid molecular beam epitaxy. *Phys. Status Solidi RRL.* **8**(11), 917 (2014)
125. T. Truttmann, A. Prakash, J. Yue, T.E. Mates, B. Jalan, Dopant solubility and charge compensation in La-doped SrSnO<sub>3</sub> films. *Appl. Phys. Lett.* **115**(15), 152103 (2019)
126. T.K. Truttmann, F. Liu, J. Garcia-Barriocanal, R.D. James, B. Jalan, Strain relaxation via phase transformation in high-mobility SrSnO<sub>3</sub> films. *ACS Appl. Electron. Mater.* **3**(3), 1127 (2021)
127. T. Wang, A. Prakash, Y. Dong, T. Truttmann, A. Bucsek, R. James, D.D. Fong, J.-W. Kim, P.J. Ryan, H. Zhou, T. Birol, B. Jalan, Engineering SrSnO<sub>3</sub> phases and electron mobility at room temperature using epitaxial strain. *ACS Appl. Mater. Interfaces.* **10**(50), 43802 (2018)
128. E.S. Hellman, E.H. Hartford, Effects of oxygen on the sublimation of alkaline earths from effusion cells. *J. Vac. Sci. Technol. B.* **12**(2), 1178 (1994)
129. Y.-S. Kim, N. Bansal, S. Oh, Simple self-gettering differential-pump for minimizing source oxidation in oxide-MBE environment. *J. Vac. Sci. Technol. A.* **29**(4), 041505 (2011)
130. Y.-S. Kim, N. Bansal, S. Oh, Crucible aperture: an effective way to reduce source oxidation in oxide molecular beam epitaxy process. *J. Vac. Sci. Technol. A.* **28**(4), 600 (2010)
131. W. Braun, J. Mannhart, Film deposition by thermal laser evaporation. *AIP Adv.* **9**(8), 085310 (2019)
132. I. Sadeghi, K. Ye, M. Xu, J.M. LeBeau, R. Jaramillo, Making BaZrS<sub>3</sub> chalcogenide perovskite thin films by molecular beam epitaxy. *Adv. Funct. Mater.* 2105563 (2021).
133. M. Brahlek, G. Rimal, J.M. Ok, D. Mukherjee, A.R. Mazza, Q. Lu, H.N. Lee, T.Z. Ward, R.R. Unocic, G. Eres, S. Oh, Growth of metallic delafossite PdCoO<sub>2</sub> by molecular beam epitaxy. *Phys. Rev. Mater.* **3**(9), 093401 (2019)
134. Y.F. Nie, P. King, C. Kim, M. Uchida, H. Wei, B.D. Faeth, J. Ruf, J. Ruff, L. Xie, X. Pan, C. Fennie, D. Schlom, K. Shen, Interplay of spin-orbit interactions, dimensionality, and octahedral rotations in semimetallic SrIrO<sub>3</sub>. *Phys. Rev. Lett.* **114**(1), 016401 (2015)
135. H.P. Nair, Y. Liu, J.P. Ruf, N.J. Schreiber, S.-L. Shang, D.J. Baek, B.H. Goodge, L.F. Kourkoutis, Z.-K. Liu, K.M. Shen, D.G. Schlom, Synthesis science of SrRuO<sub>3</sub> and CaRuO<sub>3</sub> epitaxial films with high residual resistivity ratios. *APL Mater.* **6**(4), 046101 (2018)
136. M. Uchida, T. Nomoto, M. Musashi, R. Arita, M. Kawasaki, Superconductivity in Uniquely Strained RuO<sub>2</sub> Films. *Phys. Rev. Lett.* **125**(14), 147001 (2020)
137. J.P. Ruf, H. Paik, N.J. Schreiber, H.P. Nair, L. Miao, J.K. Kawasaki, J.N. Nelson, B.D. Faeth, Y. Lee, B.H. Goodge, B. Pamuk, C.J. Fennie, L.F. Kourkoutis, D.G. Schlom, K.M. Shen, Strain-stabilized superconductivity. *Nat. Commun.* **12**(1), 1 (2021)
138. J.C. Bean, E.A. Sadowski, Silicon MBE apparatus for uniform high-rate deposition on standard format wafers. *J. Vac. Sci. Technol.* **20**(2), 137 (1982)
139. T. Sonoda, M. Ito, M. Kobiki, K. Hayashi, S. Takamiya, S. Mitsui, Ultra-high throughput of GaAs and (AlGa)As layers grown by MBE with a specially designed MBE system. *J. Cryst. Growth.* **95**(1–4), 317 (1989)
140. K. Kushi, H. Sasamoto, D. Sugihara, S. Nakamura, A. Kikuchi, K. Kishino: High speed growth of device quality GaN and InGaN by RF-MBE. *Mater. Sci. Eng., B.* **59**(1–3), 65 (1999).
141. P. Vogt, F.V. Hensling, K. Azizie, C.S. Chang, D. Turner, J. Park, J.P. McCandless, H. Paik, B.J. Bocklund, G. Hoffman, O. Bierwagen, D. Jena, H.G. Xing, S. Mou, D.A. Muller, S.-L. Shang, Z.-K. Liu, D.G. Schlom, Adsorption-controlled growth of Ga<sub>2</sub>O<sub>3</sub> by suboxide molecular-beam epitaxy. *APL Mater.* **9**(3), 031101 (2021)
142. J. Lapano, M. Brahlek, L. Zhang, J. Roth, A. Pogrebnnyakov, R. Engel-Herbert, Scaling growth rates for perovskite oxide virtual substrates on silicon. *Nature Commun.* **10**(1), 1 (2019)
143. A.P.N. Tchiomo, W. Braun, B.P. Doyle, W. Sigle, P. van Aken, J. Mannhart, P. Ngabonziza, High-temperature-grown buffer layer boosts electron mobility in epitaxial La-doped BaSnO<sub>3</sub>/SrZrO<sub>3</sub> heterostructures. *APL Mater.* **7**(4), 041119 (2019)
144. J. Shin, Y.M. Kim, Y. Kim, C. Park, K. Char, High mobility BaSnO<sub>3</sub> films and field effect transistors on non-perovskite MgO substrate. *Appl. Phys. Lett.* **109**(26), 262102 (2016)
145. J. Shiogai, K. Nishihara, K. Sato, A. Tsukazaki, Improvement of electron mobility in La:BaSnO<sub>3</sub> thin films by insertion of an atomically flat insulating (Sr, Ba)SnO<sub>3</sub> buffer layer. *AIP Adv.* **6**(6), 065305 (2016)
146. H.J. Kim, U. Kim, T.H. Kim, J. Kim, H.M. Kim, B.-G. Jeon, W.-J. Lee, H.S. Mun, K.T. Hong, J. Yu, K. Char, K.H. Kim, Physical properties of transparent perovskite oxides (Ba, La)SnO<sub>3</sub> with high electrical mobility at room temperature. *Phys. Rev. B.* **86**(16), 165205 (2012)
147. E. McCalla, D. Phelan, M.J. Krogstad, B. Dabrowski, C. Leighton, Electrical transport, magnetic, and thermodynamic properties of La-, Pr-, and Nd-doped BaSnO<sub>3-δ</sub> single crystals. *Phys. Rev. Mater.* **2**(8), 084601 (2018)
148. Z. Galazka, R. Uecker, K. Irmscher, D. Klimm, R. Bertram, A. Kwasniewski, M. Naumann, R. Schewski, M. Pietsch, U. Juda, A. Fiedler, M. Albrecht, S. Ganschow, T. Markurt, C. Guguschev, M. Bickermann, Melt growth and properties of bulk BaSnO<sub>3</sub> single crystals. *J. Condens. Matter Phys.* **29**(7), 075701 (2016)

149. E.H. Mountstevens, J.P. Attfield, S.A.T. Redfern, Cation-size control of structural phase transitions in tin perovskites. *J. Condens. Matter Phys.* **15**(49), 8315 (2003)
150. R. Uecker, R. Bertram, M. Brützmam, Z. Galazka, T.M. Gesing, C. Guguschev, D. Klimm, M. Klupsch, A. Kwasniewski, D.G. Schlom, Large-lattice-parameter perovskite single-crystal substrates. *J. Cryst. Growth.* **457**, 137 (2017)
151. C. Guguschev, D. Klimm, M. Brützmam, T.M. Gesing, M. Gogolin, H. Paik, A. Dittmar, V.J. Fratello, D.G. Schlom, Single crystal growth and characterization of  $\text{Ba}_2\text{ScNbO}_6$ —a novel substrate for  $\text{BaSnO}_3$  films. *J. Cryst. Growth.* **528**, 125263 (2019)
152. S. Yu, D. Yoon, J. Son, Enhancing electron mobility in La-doped  $\text{BaSnO}_3$  thin films by thermal strain to annihilate extended defects. *Appl. Phys. Lett.* **108**(26), 262101 (2016)
153. H.J. Cho, T. Onozato, M. Wei, A. Sanchela, H. Ohta, Effects of vacuum annealing on the electron mobility of epitaxial La-doped  $\text{BaSnO}_3$  films. *APL Mater.* **7**(2), 022507 (2018)
154. H.M. Kim, U. Kim, C. Park, H. Kwon, K. Char, Thermally stable pn-junctions based on a single transparent perovskite semiconductor  $\text{BaSnO}_3$ . *APL Mater.* **4**(5), 056105 (2016)
155. J. Wang, B. Luo, Electronic properties of p-type  $\text{BaSnO}_3$  thin films. *Ceram. Int.* **46**(16, Part A), 25678 (2020).
156. M. Glerup, K.S. Knight, F.W. Poulsen, High temperature structural phase transitions in  $\text{SrSnO}_3$  perovskite. *Mater. Res. Bull.* **40**(3), 507 (2005)
157. M.C.F. Alves, S. Boursicot, S. Ollivier, V. Bouquet, S. Députier, A. Perrin, I.T. Weber, A.G. Souza, I.M.G. Santos, M. Guilloux-Viry, Synthesis of  $\text{SrSnO}_3$  thin films by pulsed laser deposition: influence of substrate and deposition temperature. *Thin Solid Films* **519**(2), 614 (2010)
158. Q. Liu, J. Dai, X. Zhang, G. Zhu, Z. Liu, G. Ding, Perovskite-type transparent and conductive oxide films: Sb- and Nd-doped  $\text{SrSnO}_3$ . *Thin Solid Films* **519**(18), 6059 (2011)
159. E. Baba, D. Kan, Y. Yamada, M. Haruta, H. Kurata, Y. Kanemitsu, Y. Shimakawa, Optical and transport properties of transparent conducting La-doped  $\text{SrSnO}_3$  thin films. *J. Phys. D* **48**(45), 455106 (2015)
160. Q. Liu, F. Jin, G. Gao, W. Wang, Ta doped  $\text{SrSnO}_3$  epitaxial films as transparent conductive oxide. *J. Alloys Compd.* **717**, 62 (2017)
161. Q. Gao, H. Chen, K. Li, Q. Liu, Band gap engineering and room-temperature ferromagnetism by oxygen vacancies in  $\text{SrSnO}_3$  epitaxial films. *ACS Appl. Mater. Interfaces.* **10**(32), 27503 (2018)
162. Q. Gao, K. Li, L. Zhao, K. Zhang, H. Li, J. Zhang, Q. Liu, Wide-range band-gap tuning and high electrical conductivity in La- and Pb-doped  $\text{SrSnO}_3$  epitaxial films. *ACS Appl. Mater. Interfaces.* **11**(28), 25605 (2019)
163. K. Li, Q. Gao, L. Zhao, Q. Liu, Electrical and optical properties of Nb-doped  $\text{SrSnO}_3$  epitaxial films deposited by pulsed laser deposition. *Nanoscale Res. Lett.* **15**(1), 164 (2020)
164. M. Wei, H.J. Cho, H. Ohta, Tuning of the optoelectronic properties for transparent oxide semiconductor  $\text{ASnO}_3$  by modulating the size of A-ions. *ACS Appl. Electron. Mater.* **2**(12), 3971 (2020)
165. M. Wei, A.V. Sanchela, B. Feng, Y. Ikuhara, H.J. Cho, H. Ohta, High electrical conducting deep-ultraviolet-transparent oxide semiconductor La-doped  $\text{SrSnO}_3$  exceeding  $\sim 3000 \text{ S cm}^{-1}$ . *Appl. Phys. Lett.* **116**(2), 022103 (2020)
166. T.K. Truttman, J.-J. Zhou, I.-T. Lu, A.K. Rajapitamahuni, F. Liu, M. Bernardi, T. Mates, B. Jalan: Combined Experimental-Theoretical Study of Electron Mobility-Limiting Mechanisms in  $\text{SrSnO}_3$ . *Unpublished manuscript* (2021)
167. K. Nam, J. Li, M. Nakarmi, J. Lin, H. Jiang, Achieving highly conductive AlGaIn alloys with high Al contents. *Appl. Phys. Lett.* **81**(6), 1038 (2002)
168. B. Borisov, V. Kuryatkov, Y. Kudryatsev, R. Asomoza, S. Nikishin, D. Song, M. Holtz and H. Temkin: Si-doped  $\text{Al}_x\text{Ga}_{1-x}\text{N}$  ( $0.56 \leq x \leq 1$ ) layers grown by molecular beam epitaxy with ammonia. *Appl. Phys. Lett.* **87**(13), 132106 (2005).
169. R. Collazo, S. Mita, J. Xie, A. Rice, J. Tweedie, R. Dalmau, Z. Sitar, Progress on n-type doping of AlGaIn alloys on AlN single crystal substrates for UV optoelectronic applications. *Phys. Status Solidi C.* **8**(7–8), 2031 (2011)
170. M. Nakarmi, K. Kim, K. Zhu, J. Lin and H. Jiang: Transport properties of highly conductive n-type Al-rich  $\text{Al}_x\text{Ga}_{1-x}\text{N}$  ( $x \geq 0.7$ ). *Appl. Phys. Lett.* **85**(17), 3769 (2004).
171. I. Bryan, Z. Bryan, S. Washiyama, P. Reddy, B. Gaddy, B. Sarkar, M.H. Breckenridge, Q. Guo, M. Bobea, J. Tweedie, Doping and compensation in Al-rich AlGaIn grown on single crystal AlN and sapphire by MOCVD. *Appl. Phys. Lett.* **112**(6), 062102 (2018)
172. T. Ive, O. Brandt, H. Kostial, K.J. Friedland, L. Däweritz, K.H. Ploog, Controlled n-type doping of AlN: Si films grown on 6H-SiC (0001) by plasma-assisted molecular beam epitaxy. *Appl. Phys. Lett.* **86**(2), 024106 (2005)
173. M. Baldini, M. Albrecht, A. Fiedler, K. Irmscher, R. Schewski, G. Wagner, Si- and Sn-doped homoepitaxial  $\beta\text{-Ga}_2\text{O}_3$  layers grown by MOVPE on (010)-oriented substrates. *ECS J. Solid State Sci. Technol.* **6**(2), Q3040 (2016)
174. L.R. Thoutam, J. Yue, A. Prakash, T. Wang, K.E. Elangovan, B. Jalan, Electrostatic control of insulator-metal transition in La-doped  $\text{SrSnO}_3$  films. *ACS Appl. Mater. Interfaces.* **11**(8), 7666 (2019)
175. J. Yue, A. Prakash, M.C. Robbins, S.J. Koester, B. Jalan, Depletion mode MOSFET using La-doped  $\text{BaSnO}_3$  as a channel material. *ACS Appl. Mater. Interfaces.* **10**(25), 21061 (2018)
176. V.S.K. Chaganti, A. Prakash, J. Yue, B. Jalan, S.J. Koester, Demonstration of a depletion-mode  $\text{SrSnO}_3$  n-channel MESFET. *IEEE Electron Device Lett.* **39**(9), 1381 (2018)
177. V.S.K. Chaganti, T.K. Truttman, F. Liu, B. Jalan, S.J. Koester,  $\text{SrSnO}_3$  field-effect transistors with recessed gate electrodes. *IEEE Electron Device Lett.* **41**(9), 1428 (2020)

178. J. Wen, V.S.K. Chaganti, T.K. Truttman, F. Liu, B. Jalan, S.J. Koester, SrSnO<sub>3</sub> metal-semiconductor field-effect transistor with GHz operation. *IEEE Electron Device Lett.* **42**(1), 74 (2020)
179. S. Wemple, Some transport properties of oxygen-deficient single-crystal potassium tantalate (KTaO<sub>3</sub>). *Phys. Rev.* **137**(5A), A1575 (1965)
180. K. Ueno, S. Nakamura, H. Shimotani, H. Yuan, N. Kimura, T. Nojima, H. Aoki, Y. Iwasa, M. Kawasaki, Discovery of superconductivity in KTaO<sub>3</sub> by electrostatic carrier doping. *Nat. Nanotechnol.* **6**(7), 408 (2011)
181. C. Liu, X. Yan, D. Jin, Y. Ma, H.-W. Hsiao, Y. Lin, T.M. Bretz-Sullivan, X. Zhou, J. Pearson, B. Fisher, J.S. Jiang, W. Han, J.-M. Zuo, J. Wen, D.D. Fong, J. Sun, H. Zhou, A. Bhattacharya, Two-dimensional superconductivity and anisotropic transport at KTaO<sub>3</sub> (111) interfaces. *Science* **371**, 716 (2021)
182. F. Gitmans, Z. Sitar, P. Günter, Growth of tantalum oxide and lithium tantalate thin films by molecular beam epitaxy. *Vacuum* **46**(8), 939 (1995)
183. Patrick Gemperline, S. Thapa, S. Provence and R.B. Comes: Spin-Orbit Coupled 2-Dimensional Electron Gases in SrTaO<sub>3</sub> Heterostructures. <https://meetings.aps.org/Meeting/MAR21/Session/P55.12>. (2021).
184. L. Weston, L. Bjaalie, K. Krishnaswamy, C. Van de Walle, Origins of n-type doping difficulties in perovskite stannates. *Phys. Rev. B.* **97**(5), 054112 (2018)
185. Z. Yan, H. Takei, H. Kawazoe, Electrical conductivity in transparent ZnGa<sub>2</sub>O<sub>4</sub>: reduction and surface-layer structure transformation. *J. Am. Ceram. Soc.* **81**(1), 180 (1998)
186. S.K. Sampath, J.F. Cordaro, Optical properties of zinc aluminate, zinc gallate, and zinc aluminogallate spinels. *J. Am. Ceram. Soc.* **81**(3), 649 (1998)
187. Z. Galazka, S. Ganschow, R. Schewski, K. Irmscher, D. Klimm, A. Kwasniewski, M. Pietsch, A. Fiedler, I. Schulze-Jonack, M. Albrecht, T. Schröder, M. Bickermann, Ultra-wide bandgap, conductive, high mobility, and high quality melt-grown bulk ZnGa<sub>2</sub>O<sub>4</sub> single crystals. *APL Mater.* **7**(2), 022512 (2019)
188. Z. Galazka, D. Klimm, K. Irmscher, R. Uecker, M. Pietsch, R. Bertram, M. Naumann, M. Albrecht, A. Kwasniewski, R. Schewski, M. Bickermann, MgGa<sub>2</sub>O<sub>4</sub> as a new wide bandgap transparent semiconducting oxide: growth and properties of bulk single crystals. *Phys. Status Solidi A.* **212**(7), 1455 (2015)
189. B. Thielert, C. Janowitz, Z. Galazka, M. Mulazzi, Theoretical and experimental investigation of the electronic properties of the wide band-gap transparent semiconductor MgGa<sub>2</sub>O<sub>4</sub>. *Phys. Rev. B.* **97**(23), 235309 (2018)
190. Y. Jang, S. Hong, J. Seo, H. Cho, K. Char, Z. Galazka, Thin film transistors based on ultra-wide bandgap spinel ZnGa<sub>2</sub>O<sub>4</sub>. *Appl. Phys. Lett.* **116**(20), 202104 (2020)
191. M. Sousa, C. Rossel, C. Marchiori, H. Siegart, D. Caimi, J.P. Locquet, D.J. Webb, R. Germann, J. Fompeyrine, K. Babich, J.W. Seo, C. Dieker, Optical properties of epitaxial SrHfO<sub>3</sub> thin films grown on Si. *J. Appl. Phys.* **102**(10), 104103 (2007)
192. T. Tsurumi, T. Harigai, D. Tanaka, S.-M. Nam, H. Kakemoto, S. Wada, K. Saito, Artificial ferroelectricity in perovskite superlattices. *Appl. Phys. Lett.* **85**(21), 5016 (2004)
193. C. Rossel, B. Mereu, C. Marchiori, D. Caimi, M. Sousa, A. Guiller, H. Siegart, R. Germann, J.P. Locquet, J. Fompeyrine, D.J. Webb, C. Dieker, J.W. Seo, Field-effect transistors with SrHfO<sub>3</sub> as gate oxide. *Appl. Phys. Lett.* **89**(5), 053506 (2006)
194. Z. Zhong, P. Hansmann, Band alignment and charge transfer in complex oxide interfaces. *Phys. Rev. X.* **7**(1), 011023 (2017)
195. R. Engel-Herbert, Y. Hwang, J. Cagnon, S. Stemmer, Metal-oxide-semiconductor capacitors with ZrO<sub>2</sub> dielectrics grown on In<sub>0.53</sub>Ga<sub>0.47</sub>As by chemical beam deposition. *Appl. Phys. Lett.* **95**(6), 062908 (2009)
196. Y. Hwang, V. Chobpattana, J.Y. Zhang, J.M. LeBeau, R. Engel-Herbert, S. Stemmer, Al-doped HfO<sub>2</sub>/In<sub>0.53</sub>Ga<sub>0.47</sub>As metal-oxide-semiconductor capacitors. *Appl. Phys. Lett.* **98**(14), 142901 (2011)
197. A.P. Kajdos, D.G. Ouellette, T.A. Cain, S. Stemmer, Two-dimensional electron gas in a modulation-doped SrTiO<sub>3</sub>/Sr(Ti, Zr)O<sub>3</sub> heterostructure. *Appl. Phys. Lett.* **103**(8), 082120 (2013)
198. H. Mizoguchi, P.M. Woodward, S.-H. Byeon, J.B. Parise, Polymorphism in NaSbO<sub>3</sub>: structure and bonding in metal oxides. *J. Am. Chem. Soc.* **126**(10), 3175 (2004)
199. K.H. Zhang, K. Xi, M.G. Blamire, R.G. Egdell, P-type transparent conducting oxides. *J. Condens. Matter Phys.* **28**(38), 383002 (2016)
200. D. Shin, J. Foord, R. Egdell, A. Walsh, Electronic structure of CuCrO<sub>2</sub> thin films grown on Al<sub>2</sub>O<sub>3</sub> (001) by oxygen plasma assisted molecular beam epitaxy. *J. Appl. Phys.* **112**(11), 113718 (2012)
201. G. Jellison Jr., I. Paulauskas, L. Boatner, D. Singh, Optical functions of KTaO<sub>3</sub> as determined by spectroscopic ellipsometry and comparison with band structure calculations. *Phys. Rev. B.* **74**(15), 155130 (2006)
202. T. Zhang, K. Zhao, J. Yu, J. Jin, Y. Qi, H. Li, X. Hou, G. Liu, Photocatalytic water splitting for hydrogen generation on cubic, orthorhombic, and tetragonal KNbO<sub>3</sub> microcubes. *Nanoscale* **5**(18), 8375 (2013)
203. E. Chikoidze, C. Sartet, I. Madaci, H. Mohamed, C. Vilar, B. Ballesteros, F. Belarre, E. del Corro, P. Vales-Castro, G. Sauthier, L. Li, M. Jennings, V. Sallet, Y. Dumont, A. Pérez-Tomás, p-type ultrawide-band-gap spinel ZnGa<sub>2</sub>O<sub>4</sub>: new perspectives for energy electronics. *Cryst. Growth Des.* **20**(4), 2535 (2020)
204. L. Bjaalie, B. Himmetoglu, L. Weston, A. Janotti, C. Van de Walle, Oxide interfaces for novel electronic applications. *New J. Phys.* **16**(2), 025005 (2014)